DISCRETE FRACTURE NETWORK MODELING AND GEL INJECTION SIMULATION IN FRACTURED CARBONATES

A THESIS SUBMITTED TO
THE GRADUATE SCHOOL OF NATURAL AND APPLIED SCIENCES
OF
MIDDLE EAST TECHNICAL UNIVERSITY

BY

ASHKAN SOLTANIEH

IN PARTIAL FULFILLMENT OF THE REQUIREMENTS
FOR
THE DEGREE OF MASTER OF SCIENCE
IN
PETROLEUM AND NATURAL GAS ENGINEERING

JANUARY 2015

Approval of the Thesis:

DISCRETE FRACTURE NETWORK MODELING AND GEL INJECTION SIMULATION IN FRACTURED CARBONATES

submitted by **ASHKAN SOLTANIEH** in partial fulfillment of the requirements for the degree of **Master of Science in Petroleum and Natural Gas Engineering Department, Middle East Technical University** by,

Prof. Dr. Gülbin Dural Ünver
Dean, Graduate School of **Natural and Applied Sciences** _____

Prof. Dr. Mahmut Parlaktuna
Head of Department, **Petroleum and Natural Gas Engineering** _____

Prof. Dr. Serhat Akın
Supervisor, **Petroleum and Natural Gas Engineering Dept., METU** _____

Examining Committee Members:

Prof. Dr. Mahmut Parlaktuna
Petroleum and Natural Gas Engineering Dept., METU _____

Prof. Dr. Serhat Akın
Petroleum and Natural Gas Engineering Dept., METU _____

Can Sungu Bakiler, M.Sc.
Petroleum and Natural Gas Engineering Dept., METU _____

Kubilay Kumsal, Ph.D.
Consultant, Valuera Energy Inc. _____

Murat Demir, M.Sc.
Senior Reservoir Engineer, Turkish Petroleum Co. _____

Date: 16.01.2015

I hereby declare that all information in this document has been obtained and presented in accordance with academic rules and ethical conduct. I also declare that, as required by these rules and conduct, I have fully cited and referenced all material and results that are not original to this work.

Name, Last name: Ashkan Soltanieh

Signature:

ABSTRACT

DISCRETE FRACTURE NETWORK MODELING AND GEL INJECTION SIMULATION IN FRACTURED CARBONATES

Soltanieh, Ashkan

M.S., Department of Petroleum and Natural Gas Engineering

Supervisor: Prof. Dr. Serhat Akin

January 2015, 67 pages

Discrete Fracture Network (DFN) model is a recently developed, efficient approach to model fractured reservoirs. This model directly takes into account the geometry as well as conductivity and connectivity of fractures forming a network. It is a special tool that considers fluid flow and transport processes in fractured rock masses through a system of connected fractures. Because of fractured nature of carbonate reservoirs, hydrocarbon production is usually restricted by excess water production. Polymer gel injection can be considered as a method to shutoff fracture conduits in water bearing zones. In this study, a highly fractured heavy oil reservoir going through polymer injection is modeled using DFN approach where it is used as a tool for upscaling fracture properties to the dual-porosity fluid flow simulator. DFN model is created by conditioning the model set to some available fracture parameters. The rest of the parameters are estimated by stochastic correlations to existing fracture parameters. The model is then validated by conditioning it to well test data obtained from a heavily fractured field located in South East Turkey. A CMG STARS single well/dual-porosity numerical model whose fracture properties are populated by the DFN model results is used to model polymer injection. It is observed that the matches obtained with DFN populated dual porosity model is acceptable. Finally, scenarios studies were conducted to identify and optimize polymer gel injection parameters.

Keywords: Discrete Fracture Network Modeling, DFN, Water Shutoff Gels

ÖZ

ÇATLAKLI KARBONATLARDA AYRIK ÇATLAK AĞI MODELİ VE JEL ENJEKSİYONU SİMÜLASYONU

Soltanieh, Ashkan
Yüksek Lisans, Petrol ve Doğal Gaz Mühendisliği Bölümü
Tez Yöneticisi: Prof. Dr. Serhat Akın
Ocak 2015, 67 sayfa

Çatlaklı rezervuarları verimli şekilde modelleyebilmek için Ayrık Çatlak Ağı (AÇA) son zamanlarda geliştirilmiştir. Bu model çatlakların geometrisini, iletkenliğini ve bağlantılığını göz önünde bulundurarak çatlak ağı oluşturmaktadır. Bu metot aracığıyla, birbirine bağlı çatlaklı kaya sistemindeki sıvı akışını görebilmekteyiz. Karbonat rezervuarlar genellikle çatlaklı oldukları için, hidrokarbon üretimi çoğu zaman aşırı su üretimiyle sınırlanmaktadır. Polimer jel basma, aşırı su üretim bölgelerinde çatlak yolunu kapatma metodu olarak uygulanmaktadır. Bu çalışmada çok çatlaklı ağır petrol sahasında, AÇA metodu uygulanarak çatlak ağı modellemesi ardından belirmiş olan çatlak özelliklerini kullanarak polimer jel basma simülasyonu çift yönlü-boşluklu benzetim uygulamasıyla yapılmaktadır. AÇA metodu, modeli oluştururken onu elde edilmiş olan bazı çatlak parametreleri ile sınırlamaktadır. Geriye kalan parametreler ise bilinen parametrelere korele edilerek tahmin edilmektedir. Ardından benzetim test verilerini, sahadan alınan gerçek kuyu testi verileri ile doğrulanmaktadır. Tek kuyulu/çift boşluklu CMG STARS numerik modeli ile elde edilmiş çatlak özelliklerini kullanarak polimer jel uygulaması modeli oluşturulmaktadır. Simülasyondan alınmış sonuçlardan ve gerçek sahadan alınmış veriler arasında kabuledebilir bir uyum görülmektedir. Sonuç olarak senaryo çalışmaları polimer jel basma parametrelerini tanımlama ve optimize etmek için yapılmaktadır.

Anahtar Kelimeler: Ayrık Çatlak Ağı Modellemesi, AÇA, Su Kesme Jelleri

To My Family

ACKNOWLEDGMENTS

My sincerest gratitude goes to Prof. Dr. Serhat Akın for his patience, understanding, guidance, and ready support. Your advice on both research as well as on my career have been priceless. I would also like to thank my thesis examining committee members for serving as committee members even at hardship. Personnel of production department of Turkish Petroleum Co., especially Mr. Murat Demir contribution was invaluable in obtainment of required data for simulation.

I convey my special thanks to Serdar Bender and Javid Shiriyev for their helpful involvement during this period. I would like to express my appreciations to department's assistants, specially Selin Güven, and Tuğçe Özdemir for their kind support and encouragement. Finally, my appreciation goes to Shirin for her motivation and encouragement.

TABLE OF CONTENTS

LIST OF TABLES

TABLES

LIST OF FIGURES

FIGURES

LIST OF ABBREVIATIONS

DFN	Discrete Fracture Network
EPM	Equivalent Porous Media
PIT	Total Productivity Index
Samp. S.	Sample Size
Std Dev.	Standard Deviation
Max.	Maximum
Min.	Minimum
Xlinker	Cross Linking Agent

CHAPTER 1

INTRODUCTION

Naturally Fractured Reservoirs (NFR) contain a substantial amount of the known hydrocarbons reservoirs worldwide and contribute a large extent of petroleum production. NFR can be defined as, a complex network of several fracture families with different spatial distribution and conductivity. Since naturally fractured systems comprise of two domains, i.e. rock matrix and rock fracture, performing characterization study has become a challenging task, [1]. Several approaches have been conducted by different authors to replicate the behavior of fractured reservoirs.

Warren and Root [2] idealized heterogeneous porous medium and represented the naturally fractured dual-porosity system by a stack of rectangular blocks. They developed their proposed model by employing several assumptions:

1) The rock matrix, contained within a systematic array of identical rectangular parallelepipeds, is homogeneous, isotropic, with high storativity, low permeability, and it is not a pathway for fluid to flow into the well.

2) Fractures, contained within a system of continuous, uniform, and parallel openings (fissures) that are oriented to one of the principal axes of permeability. In order to simulate proper degree of desired anisotropy, different fracture width or spacing may exist along each of the axes. Flow from matrix to fractures occurs under pseudo-steady state conditions and fractures are acting like conduits to the wellbore.

The approach of dual-porosity models, although very efficient, suffers from some significant constraints. The first limitation is, it cannot be applied to disconnected fractured media. In addition, it is not appropriate to model a small number of large-

scale fractures which may dominate the flow. Another inadequacy is difficulty in accurately evaluating the flow equation between the matrix and the fractures, [3].

For these reasons it is understood that, using a model which represent the fractures individually can overcome limitations of dual-porosity models. Therefore, it is the beginning of application of Discrete Fracture Network (DFN) models in reservoir simulation. These models, not only, explicitly take into account the geometry, but also, the conductivity and connectivity of fracture network. DFN models can be utilized as stand-alone as well as in combination with the dual-porosity approach to evaluate transfer function in this model, [3].

Some of the approaches to DFN concept are based on structural discretization scheme. For instance, Lee et al. [4] presented a hierarchical modeling of flow, where the permeability contribution of small fractures were determined from analytical expressions, and effective permeability associated with large-scale fractures were derived numerically, based on boundary element method. On the other hand, unstructured discretization schemes use finite element and control volume finite difference methods to deal with DFN concept. As an example, Juanes et al. [5] modeled single phase groundwater flow using a general finite element formulation in two and three dimensional in fractured porous media. Although, the existing approaches based on finite element procedures are successful in the case of single phase flow and heat transfer, in highly heterogeneous systems with multiphase flow they do not guarantee local mass conservation.

One of the recent approaches to discrete fracture modeling is to utilize finite volume method. In cell-based approaches, control volumes can be readily aligned with the discontinuity of permeability field. Dershowitz et al. [6], in their cell-based study on DFN modeling, used finite volume method to calculate dual porosity parameters for fractured porous medium. Karimi et al. [3] declared that in the great majority, existing reservoir simulators are based on finite difference or control volume finite difference methods. Thus, utilizing cell-based approaches are probably more appropriate for numerical reservoir simulation applications.

Although fractures are an efficient conduit for desired fluid production, they are also a pathway for unwanted fluid like water, and reduces the oil production rate due to increased water-cut from wellbore. Two primary technologies can be used to restrict water from entering the wellbore: (1) mechanical blocking devices, and (2) chemicals that shut off water-bearing channels or fractures within the formation, preventing water from making its way to the well. The first method, is achieved by using various mechanical and well construction techniques to block water from entering to the well. Mechanical approaches, however, may not be effective in solving other more complex types of water production problems i.e., water leaking from fractures with minor apertures. On the other hand, most of water shut-off chemicals are polymer gels or their pre-gel forms (gelants). In the process of selectively entering the cracks and pathways that water goes through, gel solutions displace it. Once the gels are fixed through the cracks, they block most of the water movement to the well while allowing oil to flow to the well.

Discrete fracture network modeling and polymer gel injection simulation have been conducted by several authors, separately. This study is a combination of two different approaches: DFN modeling approach and dual porosity reservoir modeling approach for history match study. The final model is the result of two simulator, i.e. cell properties from DFN modeller used as input for reservoir simulator and recovery processing analysis.

CHAPTER 2

LITERATURE REVIEW

Discontinuities or fractures in the formation are divided into four groups: Faults, Bedding planes, Joints, and Cleavage. In the context of flow and transport modeling, understanding that geological displacement can be normal to fracture wall or parallel to the fracture plane is sufficient, [7]. Among these groups, two principal classes of fractures are faults and joints. Faults are generated when identifiable shear displacement has occurred, while joints are breaks of geological origin along which there has been no visible relative displacement. Fault networks normally consist of two or three families of oriented fractures. However, joint networks consist of one to non-observable number of fractured families, [7]. Odling et al. [8] noted that joint systems often have greater intensity and composed of a number of orientation sets and well-connected alignment particularly at the outcrop scale, whereas fault maps contain less intensity and orientation, and consequently less well-connected alignment. For quantitative description of discontinuities in rock mass, nine geometrical parameters to describe the characteristics of discontinuities has been defined:, [9]

1) Orientation: The attitude of discontinuity in space.
2) Spacing: The perpendicular distance between adjacent fractures.
3) Frequency: Number of discontinuities per linear, areal, or volumetric measurement.
4) Intensity: One, two, or three dimensional measurement in linear, areal, and volumetric frequency.
5) Length: The discontinuity trace length as observed in exposures.
6) Shape: The planar form of discontinuity

7) Size: The areal extent of discontinuity and is correlated to trace length distribution.
8) Roughness: The inherent surface roughness and waviness relative to mean plane of discontinuity.
9) Aperture: The perpendicular distance between walls of discontinuity, in which the intervening space is fluid filled.

The DFN method is formed by combining geometry and discrete features of rock fractures. It considers fluid flow and transport processes in fractured rocks through a network of connected fractures. The technique was created in the 1980s for both 2D and 3D problems and has been developing continuously afterwards with many applications in any field related with geology, i.e. civil, environmental, mining, and reservoir engineering and other geoscience and geoengineering fields.

DFN model can be provided deterministically, or stochastically. In deterministic model the geometrical parameters are determined by special measurement tools, like fracture intensity measurement by formation micro-scanning logging. However, in stochastic modeling the fractures parameters estimated from statistical or fractal methods, like estimating size distribution by log-normally distribution of trace length, [10]. Modeling with deterministic measurement is more reliable than stochastic modeling method. However, due to the limitation of measurement techniques for exploring the geometry and locations of sub-surface structures, we have to use stochastic approaches to expand the range of our predictions. We must include stochastic measurements and correlations because in many cases there are sparse available data measured at limited locations. For example, there are no deterministic methods for measuring fracture size, i.e. only some stochastic methods exist to correlate it to fracture length.

2.1 Stochastic Modeling Approach

Stochastic simulation of fractured systems utilizes Probability Density Functions (PDFs) of geometric parameters of fractures formulated according to field mapping results. Direct field mapping can only be conducted at surface exposures of limited size, also boreholes of limited diameter, length, and depth, and similarly on the walls

of underground excavations, i.e. tunnels, caverns, shafts, etc. of more limited measurement space and with cut-off limits for mapping. Thus, the reliability of fracture network information depends on the quality of mapping and sampling. Although direct evaluation of reliability and adequacy of individual geometric parameters is difficult, they are some dynamic analysis methods to evaluate stochastic DFN model altogether. One of the methods that is used frequently in computer DFN simulators is discussed further.

2.2 Data Attainment for DFN Modeling

It is obvious that if deterministic measurement of geometrical parameters is possible and available, stochastic determination methods is not used. Many authors have introduced different stochastic methods to distribute statistically the deterministic measurements or correlate geometrical parameters to each other. Therefore, the most recent DFN models are combination of deterministic and stochastic methods.

2.2.1 Fracture orientation

Orientation of discontinuities can be measured from cores or from exposures using one or two dimensional scanlines. The measured orientation data (poles) is plotted on stereonets.

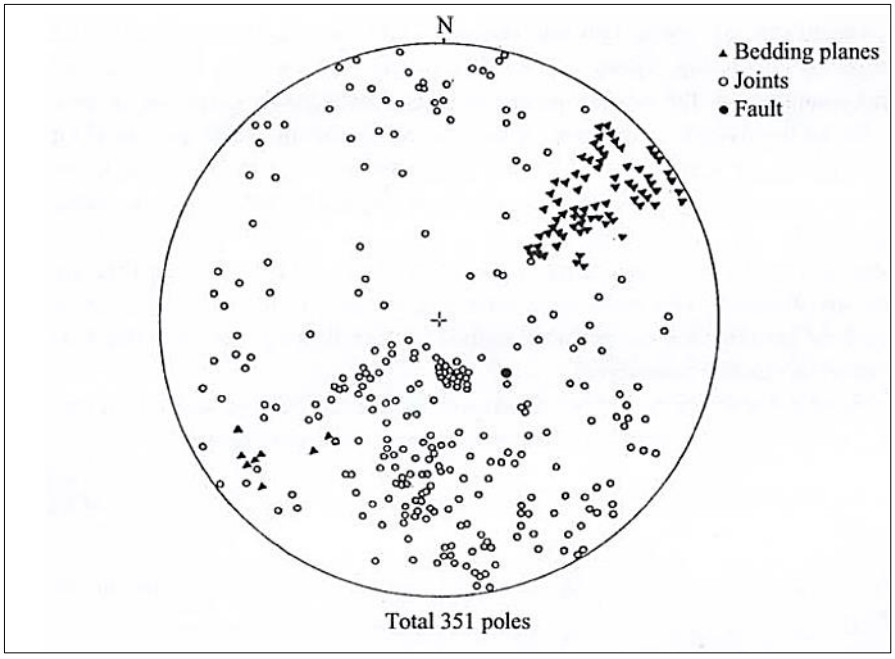

Figure 2-1**:** Plot of poles of 351 discontinuities [11]

A number of algorithms which are based on statistical approaches can be used for numerically clustering orientation data. After determining the pole concentration, mean orientation of number of discontinuities can be calculated from directional cosines.

Several probability distributions have been suggested in the literature to represent the discontinuity orientations in fracture network models, such as hemispherical uniform, Fisher, bivariate Fisher, Bingham, bivariate normal, and bivariate lognormal, [12].

2.2.2 Fracture intensity

Intensity can be expressed as different measures conducted in one, two or three dimensions. For example, fracture spacing, linear, areal, and volumetric frequency, or fracture length per unit area, and fracture area per unit volume of rock mass. Fracture intensity is often expressed in terms of areal or volumetric frequency. Dershowitz and Herda [13] provided a table of different fracture intensity measures. Table 2-1 lists their interpretation of fracture intensity.

Table 2-1: Different measures of discontinuity intensity [13]

		Dimension of sampling region		
		1. Line (Scanline or borehole)	2. Area (Rock exposure)	3. Volume (Rock mass)
Measured parameter	Number of fractures	P_{10} or λ Number of discontinuities per unit length of sampling line [L^{-1}]	P_{20} or λ_a Number of discontinuities per unit area of sampling line [L^{-2}]	P_{30} or λ_v Number of discontinuities per unit volume of sampling line [L^{-3}]
	Dimension one less than that of sampling region		P_{21} length of discontinuity per unit area of rock exposure [L^{-1}]	P_{32} Area of discontinuities per unit volume of rock exposure [L^{-1}]
	Dimension equal to that of sampling region			P_{33} Volume of discontinuities per unit volume of rock exposure [-]

2.2.3 Fracture trace length

Fracture trace length is an important parameter for describing fracture areal extent or size. Three different sampling methods are used according to size bias, truncation bias and censoring bias. In size bias measurement, larger fractures are likely to be sampled than smaller ones. In truncation bias method, trace length below some known cut-off length is not recorded. In censoring bias method, long exposure which may extend beyond the visible exposure is taken into consideration without one end or both end seen. Furthermore, orientation bias, which considers the dependence between relative orientation of rock face and fracture, and probability of a fracture appearing, is also taken into account in three dimensional simulation. [12]

2.2.4 Fracture shape

Although planar shape of fractures has profound effect in connectivity of fractures [14], rock mass is usually inaccessible in three-dimensions, and the real fracture shape is rarely known. Therefore, some researchers assume that fractures are thin circular discs randomly located in space, like study of Kulatilake and Wang [15] over three dimensional analysis of finite sized fractures . Although, some authors

assume that the pattern of differently oriented fractures are similar, Warburton [16] defined fractures in a set as parallelograms of various sizes.

2.2.5 Fracture size

Fracture size is inferred by correlating to trace length distribution obtained from straight scanline sampling [16], circular window sampling [17], and most recent method is the assumption of elliptical trace with known length as depicted in Fıgure 2-2, [18].

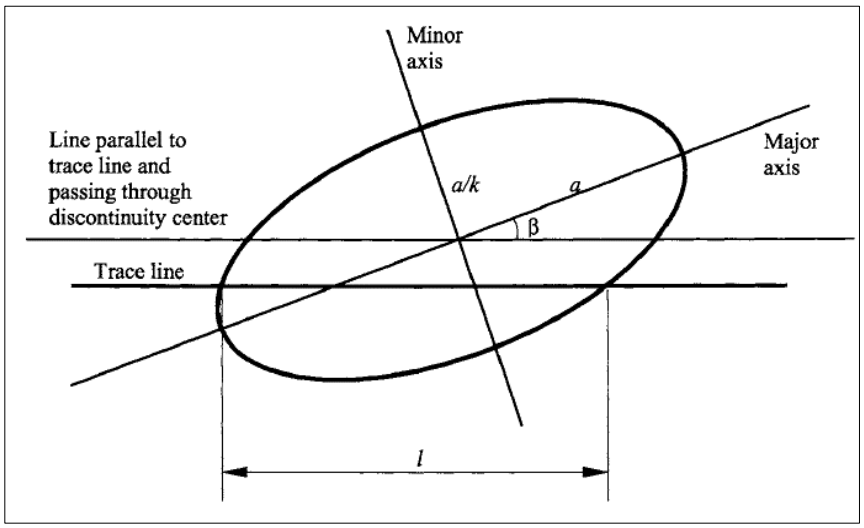

Figure 2-2: Parameters used in the definition of an elliptical discontinuity [12]

Figure 2-2 illustrates the determination of size distribution according to trace length distribution. Mean and standard and standard deviation of discontinuity size '*a'* can be determined from mean and standard deviation of trace length, '*l'*. Zhang et al. [18] suggested three distribution functions for determination of mean and standard deviation, namely, lognormal, negative exponential, and gamma distributions.

2.2.6 Fracture aperture, transmissivity, and storativity

According to literature, aperture can be measured from the width of a filled fracture. One of the tools for measurement of fracture aperture is resistivity imaging devices. The distorted and concentrated emitted currents around fractures with filled mud, are functions of fracture aperture. However, due to fracture wall roughness, gauge, degree of mineral infill and lateral continuity, it is difficult to truly determine a fracture aperture within a rock body, [19]. Fracture transmissivity can be determined

by applying reformed cubic law equation (2-1), which correlates it to cube of aperture, and assumes that the flow through fracture is laminar, viscous, and occurred between two parallel smooth planes. Thiem equation (2-2) is another correlation for determination of transmissivity. This analytical equation is based on porous media conceptualization and single well injection test or one injection, two monitoring well test. It assumes that fluid flow occurs through fractures which are in infinite areal extent, homogeneous, isotropic, and confined to a uniform thickness, [20]. Similarly, storativity can analytically be correlated to fracture aperture, based on equation (2-3). Rutqvist et al. [21] provide a linear function which interprets storativity as a function of aperture. This function is obtained from single well high pressure injection test. The assumptions of radial flow, and flowing through two parallel plane with some stiffness needed to be considered for application of storativity function.

$$T = \frac{\rho g N}{12\mu} \cdot b^3 \qquad (2\text{-}1)$$

$$T = \frac{q}{2\pi\Delta h} \cdot \ln\left(\frac{r_2}{r_1}\right) \qquad (2\text{-}2)$$

$$S = \rho g\left(\frac{A\alpha}{\sigma_n^2} + C_f b\right) \qquad (2\text{-}3)$$

In equation (2-1) ρ is density, g is gravitational acceleration, N is number of fractures that are hydraulically active, and μ is viscosity. In Equation (2-2) q is the flow rate, and Δh is difference between two observed head. r_2 in single well test is estimated radius of influence, and r_1 is well radius. In equation (2-3) A is Goodman's joint parameter, α is Biot's effective stress constant, σ_n is normal stress value, and C_f is fluid compressibility.

2.3 Equivalent Porous Media Approach to Fractures

The Equivalent Porous Media (EPM) approach defines a fractured system as a single continuum, or series of continua. In this approach, the parameter values are affected by the presence of fractures; however, the fractures are not modeled explicitly. The advantage of this approach is the requiring of only a few parameters, such as hydraulic conductivity, hydraulic gradient, effective porosity

and dispersivity for simulations, [22]. A fractured rock can be supposed to behave EPM when fracture density is increased, apertures are constant rather than distributed, orientations are distributed rather than constant, and larger sample sizes are tested. This approach does not consider the discrete parameters of fractures adequately. It fits with large number of small fractures in reservoir quite properly, [23]. One of the drawbacks of this approach is that it is not able to model the faults and large fractures properly. Since they mostly control the fluid flow in the reservoir, in the existence of large fractures the flow model does not fit the reality.

2.4 DFN Hydrostructural Model

The DFN approach provides the three dimensional framework of discrete features, which gathers flow, transport, and the flow barriers such as faults and clayey layers, which provide partial or complete seals. This DFN conceptual model can be referred to as a discrete feature "hydrostructural descriptive model", [24]. The proper hydrostructural model should consider the role of known and unknown discrete parameters that control flow and transport. Once the DFN hydrostructural model has been implemented, and the discrete parameters of importance are known deterministically, or stochastically, the DFN can be served as solution to address specific flow and transport engineering issues of concern.

There are three methods for DFN modeling: (1) Convergence of DFN and Continuum Methods, (2) Increasing Geologic Realism, and (3) Multiple Immobile Zone Transport. The main difference between these methods is the difference in transport approaches and flow model in the fractures. The first method, considers conventional continuum (EPM) transport models to examine the role of known and unknown discrete features in controlling flow and transport. The geologic realism method, the second, implements DFN modeling by integrating geology, geophysics, and hydrogeology. The third and last method, considers the realization of interaction between mobile and immobile zones in fractured rocks, [25].

In this study the DFN model is based on 'Convergence of DFN and Continuum Methods'. This model is divided into three modeling approaches. Therefore, in the next three subsections the approaches are delineated.

2.4.1 Layered DFN/EPM model

In many geological environments, heterogeneously connected fractures occur within stratigraphic columns containing units which are best represented by continuum elements. These geological environments are preferably created by Layered DFM/EPM models. The advantage of this approach is that it is able to more accurately model the response of the groundwater table and shallow wells using continuum EPM elements, while still using the DFN for evaluating connectivity between wells in the fractured granite.

2.4.2 EPM implementation of DFN hydrostructural models

This model is divided into three parts: [25]

1) Explicit modeling of a key faults and fractures:
   This model considers the faults and highly conductive fractures, which carry the vast majority of flow and transport, explicitly. Therefore, in this model EPM model can function identical to DFN model.
2) Geostatistical simulation of faults and fractures:
   During the past ten years, advances in geostatistical modeling have made it possible to implement geostatistical models in DFN hydrostructural models. This model can reproduce and enhance DFN models. Geostatistical simulation approach to faults and fracture is achieved by:
   i) Indicator kriging: Cells can be marked based on the occurrence of fractures or flow barrier faults. The geostatistically derived property fields can be adjusted accordingly. The produced fields resemble the location and properties of the discrete features.
   ii) Co-kriging: Cell hydraulic properties can be adjusted based on a combination of both the hydraulic test results which provide permeability and storativity, and the geophysical fields which are indicators for the location of faults.
   iii) Numerical inversion: Geostatistical EPM model cell hydraulic properties can be optimized by a combined inversion of the

underlying DFN hydrostructural model, geophysical data, and hydraulic data.

3) Oda tensor approach

   The Oda's approach, firstly, generates the full, three dimensional DFN. Then, overlays an EPM grid on the fractures, and derives EPM properties for each grid cell based on the DFN contained in that cell. Oda's approach can approximate equivalent permeability tensor, and fracture tensor for a specific grid.

2.4.3 Nested EPM/DFN models

These models combine the use of DFN elements in the locations where fracture geometry is of most concern. DFN elements can be applied at intersections with boreholes and tunnels, and EPM elements can be applied at less sensitive locations. According to Dershowits et al. [25], the key to the implementation of Nested EPM/DFN models is the same as for layered EPM/DFN models.

2.5 Carbonate Reservoirs and Water Shut-off Techniques

Most carbonate reservoirs are naturally fractured and contain fractures that can range from isolated microscopic fissures to kilometer-wide collections called fracture swarms or corridors, [1]. The highly fractured nature of carbonate reservoirs, although provide a high permeable zone for hydrocarbon flow, they are pathways for water production similarly. Specially, due to water coning around the wellbore, water can easily reach the well through fractures. Two options are available to reduce water production and in dealing with wells that produce large amounts of water.

2.5.1 Mechanical blocking devices

Operators may apply various mechanical and well construction techniques to block water from entering the well. Several examples of these techniques has been proposed to restrict excess water production. Straddle packers, bridge plugs, tubing patches, cement, wellbore sand plugs, well abandonment, infill drilling, pattern flow control, and horizontal wells are typical examples which have been suggested by the authors to achieve water blocking. Seright et al. [26] recommended that mechanical

approaches can be used to block leaks in casing or water that flows between the casing and the wellbore. Mechanical approaches, however, may not be effective in solving other more complex types of water production problems. For example, when water is leaking through fractures, cement is not fluid enough to flow deep into them. For these types of water problems, water shutoff gels and gelants may produce a better result.

2.5.2 Water shut-off chemicals

Chemicals can be used to limit water from entering the wellbore. These techniques shutoff water bearing fractures within the formation and prevent water from making its way to the well. Most of water shut-off chemicals are polymer gels or their pre-gel forms (gelants). In the process of selectively entering the fractures that water follows, gel solutions displace the water. Once the gel solutions are set up in the fractures, they block most of the water movement to the well while allowing oil to flow to the well. Some of the key factors recommended for consideration with respect to gel treatment designs and operations include the following.

2.5.2.1 Chemical component ingredients

Type of polymer gel, type of crosslinking agent, type of fluid mixed with gel, are important compositions needed to be considered. Polyacrylamide polymer, microbial products, and lignosulfonates are types of polymer gels. Containing metal ion or being from organic group cross-linkers are the types of crosslinking agent. Examples for type of fluid mixed with gel are fresh water and produced water. Fluid used to mix the gel is an important composition needed to be considered.

2.5.2.2 Properties of gel

Gel properties can subject to change in different stages throughout the gel treatment. Therefore, considering the properties of gel is an important issue to have a successful gel treatment. Properties of gel can be listed as, concentration and molecular weight of polymer, degree of crosslinking, density and viscosity, and also the set-up time which influences how far the gel penetrate into the fractures.

When component ingredients and gel properties are determined, treatment procedure must be decided. Preparation of well before treatment, volume of gel to be injected, injection pressure, and injection rate have to be determined to have a successful gel treatment.

Reynolds [27] suggests using the following criteria for selecting candidate wells for gel treatment:

- Wells already shut-in or near the end of their economic life
- Significant remaining mobile oil in place
- High water-oil ratio
- High producing fluid level
- Declining oil and flat water production
- Wells associated with active natural water drive
- High-permeability contrast between oil- and water-saturated rock

There are many successful examples of gel treatment in the literature. As an example, Seright et al. [26] describe 274 gel treatments conducted in naturally fractured carbonate formations. The median water-to-oil ratio was eighty-two before the treatment, then fell to 7 shortly after the treatment, and stabilized at twenty a year or two after treatment. On average, those wells produced much less water after the treatment. Following gel treatment, the oil production increased and remained above pre-treatment levels for one to two years.

CHAPTER 3

STATEMENT OF THE PROBLEM

Understanding the behavior of the fracture networks is important to perform a proper gel injection application. The main purpose of this study is developing a model under direct consideration of fracture geometrical parameters and including heterogeneous behaviour of the fractures into the model. Modeling fractures using DFN approach not only helps to provide more realistic reservoir model, but also results in a better water shut-off simulation compared to conventional single property fracture modeling. Geocellular fracture model is generated based on available stochastic measured data. Then, calibration to production test data as well as modification of the parameters are conducted to obtain well test match. Finally, history matching and gel injection simulation on a dual porosity reservoir model containing upscaled generated fractures' properties conclude the study.

CHAPTER 4

METHODOLOGY OF STUDY

In this chapter, methodology behind the DFN and reservoir model generation is described. This chapter is divided into two sections. In the first section, static data analysis and determination of geometrical parameters to provide fracture network is analysed. Next, model calibration and adjustment of uncertain parameters until offering appropriate DFN model is studied. Finally, DFN upscaling to create grid of fracture attributes, i.e. porosity and permeability for reservoir simulation are investigated. In the second section, preparing dual-continuum model, history matching, future forecasts, and gel injection simulation are described.

4.1 Generation of DFN Model

FracMan7, a software which supports integrated assessment of fractured reservoirs from data analysis, through fracture generation, to flow simulation, is used in order to generate stochastically-determined DFNs on a log-normal statistical algorithm basis. The software approach to DFN consists of three general steps. The first step includes, analyzing the information from a variety of data sources to acquire the parameters needed for step two. These parameters are fracture locations, size, shape, orientation, flow properties, and number of distinct fracture sets. Step two is generating multiple discrete fracture networks dependent upon the results of the data analysis. Lastly in step three, the fracture networks are analysed to derive engineering information. This information includes simple geometric analysis like the computation of fracture densities, as well as complex multi-well flow simulations, [28]. Step two and three are based on a forward modeling approach which is used for iteration during calibration process.

FracMan7 has three separate algorithms for fracture generation: Enhanced Baecher, Nearest Neighbor, and Levy Lee.

4.1.1 The Enhanced Baecher algorithm

This algorithm is extended form of Baecher model. According to Baecher model, fracture centers are distributed uniformly in space, using a Poisson distribution process and generated fractures are disk shape with a given radius and orientation. It is a simple algorithm in which fractures were considered planar and finite. Enhanced Baecher model utilizes fracture shapes which are generated initially as polygons with three to sixteen sides. These polygons can be equilateral or elongated, according to aspect ratio defined by the user.

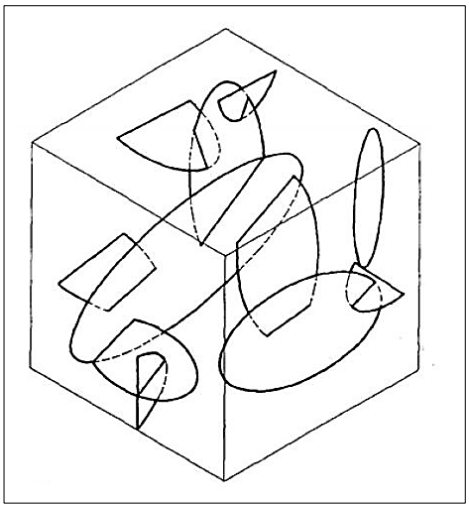

Figure 4-1: Baecher Model, [29]

In the Enhanced Baecher Model, all fractures are distributed uniformly from their center locations in space. For every fracture, FracMan7 checks whether the fracture intersects a pre-existing fracture. The portion of fracture beyond the intersection is discarded.

4.1.2 The Nearest Neighbor model

The algorithm of this model is focused on exponentially decreasing intensity of fractures, i.e. P_{32} with distance from major fractures. The magnitude of decrement is defined by user and adjustable to construct the most realistic model.

4.1.3 The Levy-Lee fractal model

This model is based on self-similar and self-affine fractal patterns. The fractal fracture patterns are simulated recursive generation scheme which utilizes self-affine transformation to produce fracture patterns from one scale to different scales. Alternatively, using 'Levy-Flight' theory one can reproduce fractal pattern according to self-similar jumps. Or, it can be generated by non-fractal procedures, then test them to determine if the resultant pattern is fractal, i.e. self-similar or self-affine. FracMan7 uses two- and three-dimensional form of one-dimensional 'Levy-Flight' model called 'Levy-Lee' model. For conversion between two- and three-dimensional models FracMan7 uses derivation method introduced by Dershowitz [28] which convert fractal mass dimension on a point located on a plane to the dimension of points in three-dimensional space required for fracture generation.

4.1.4 Field X modeling approach

Field X is one of the largest oil fields in southeastern Turkey. From structural geology point of view, it is a doubly plunging anticline. Geological analyses indicate that the field has been subjected to major tectonic events, resulting in folding, fracturing, and faulting, [30]. This field is a naturally fractured carbonate reservoir containing heavy oil, very low gas to oil ratio, and supported with a strong aquifer, [31]. Although it contributes to quite high oil production, the average water-cut exceeded 90%, recently. Using single well modeling approach, DFN model is implemented for each well reservoir section, and fracture properties for geocellular grids are executed. Four wells are modelled under assumption of square drainage boundaries determined according to available production history of each well. The selected section is divided into 600 grids (10*10*6). Finally, dual porosity reservoir model is generated as discussed in section 4.2. The schematic view of generated model fracture network is illustrated at the end of this section.

4.1.5 Determination of fracture parameters

In this part the methodology behind the determination of stochastic distribution of fracture parameters required for generating DFN model is discussed. Fracture

intensity, orientation, size, shape, and aperture distribution as well as transmissivity and storativity correlations are delineated.

4.1.5.1 Fracture intensity stochastic distribution

Spatial fracture intensity (P_{32}) is an important characteristic of a fractured rock mass. Although it can hardly ever be measured, P_{32} can be modelled based on available geological information such as spatial data of the fracture network. For modeling fracture intensity, Enhanced Baecher approach is utilized. Therefore, P_{32} under assumption of parallel fracture set can be estimated using uniform Poisson distribution of inverted fracture spacing, [32]. It has been acknowledged that the fracture spacing for each fracture set follows a negative exponential distribution [33], and according to the statistical theory the Poisson distribution can be used to model the three-dimensional fracture intensity distribution for each fracture set, [34].

For Field X the maximum and minimum fracture spacing is determined using correlation of fracture parameters to Total Productivity Index (PIT), [30]. Sener considered the following three assumptions to estimate spacing distribution from PIT variation in the field and from mapped and digitized structure depth and layer net thickness data. The first assumption involves that most fractures are concentrated in the area of maximum flexure and along the mapped fault traces. The second assumption includes, most fractures lie on nearly perpendicular planes. The third assumption is, the transmissivity of vertical fractures are equal.

FracMan7 defines intensity with Fracture count, P_{10}, P_{32}, and P_{33}, which are described in Table 2-1. According to available stochastic data and knowledge of encountering with highly fractured network system, P_{32} is considered for fracture intensity of the Field X fracture system. However, its value can subject to change during calibration process. Due to existence of multiple faults in the reservoir the proximity of wells to the faults can directly affect the number of fractures around the wellbore. Therefore, considering one single P_{32} value for whole system is not logical.

4.1.5.2 Fracture orientation stochastic distribution

Fracture orientation is defined as attitude of discontinuity in space. It is described by the dip, which is the line of the maximum declination on the fracture surface measured from the horizontal, and the dip direction or azimuth, which is measured clockwise from true north, [12]. There is no deterministic measurement of fracture orientation for Field X. Therefore, the initial distribution of fracture orientation needed to be considered under two assumptions. The first assumption is about the fracture's pole plunge direction and the second one is about the direction of pole trend. Fractures occur in the direction perpendicular to the least stress. Based on experience horizontal fractures will occur at depths less than approximately 2000 feet. The reason is the earth's overburden stress which applies the least principal stress at these depths. For regions beyond this depth, the overburden stress increases by approximately 1 psi per feet, making the overburden stress the dominant stress, and the horizontal confining stress is now the least principle stress. Therefore fractures will be oriented perpendicular in vertical direction. Field X reservoir is located at depth about 4000 feet; therefore considering this assumption for fracture orientation is reasonable. On the other hand, the reservoir section is heavily faulted and fractures most frequently occur in the direction perpendicular to the nearest fault dip direction. Therefore, the dip of fractures in the model is taken to be ninety degrees and the dip direction is taken to be perpendicular to dip direction of nearest fault on each well.

FracMan7 provides, constant, Fisher, bivariate normal, bivariate Fisher, bivariate Bingham, and elliptical Fisher distribution for fracture orientation. Enstein et al. [35] conducted goodness of fit test at 5 percent significance level for distribution results and for all of them it was observed that there is an inadequacy of currently available analytical distributions in presenting the fracture orientation. Therefore, they claimed that using empirical distributions for orientation data is more preferable. Several studies conducted on DFN modeling assume Fisher distribution for fracture orientation distribution, [36], [37], [38]. As a result, in this study fracture orientation is distributed according to Fisher distribution, which is a symmetric distribution

about the mean orientation and uses a single parameter, the Fisher constant ‘K’. The ‘K’ value describes the tightness or dispersion of fracture orientation set.

4.1.5.3 Fracture size and shape stochastic distribution

Direct measurement of fracture length in order to correlate it with fracture size to provide log-normal distributed fracture sizes is not available to the case of Field X. Therefore, size distribution is prepared by considering the layer thickness dominated modeling, and according to an arbitrary mean and variance values.

Sener [30] indicated that the fractures are assumed to be wedge-shaped. Therefore, for modeling of fracture shape in FracMan7 this assumption is conserved, and we used triangular shaped fractures.

4.1.5.4 Fracture aperture, storativity, and transmissivity stochastic distribution

Aperture distribution data is provided by Sener [30] for Field X. These data are distributed using lognormal distribution which is the most appropriate type of distribution for fracture aperture. The fracture aperture distribution for wells is plotted in Figures 4-2 and 4-3.

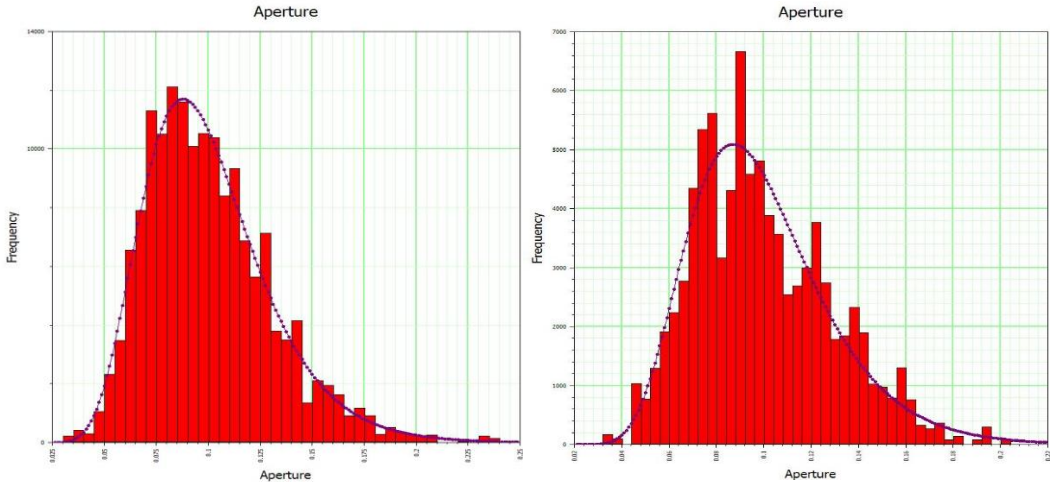

Figure 4-2: Aperture lognormal distribution for wells, 72 (left) and 137 (right)

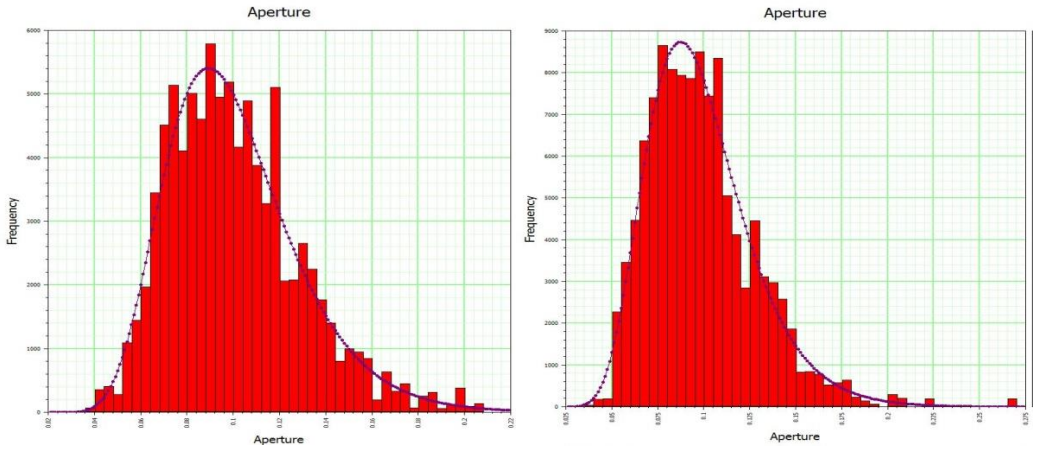

Figure 4-3: Aperture log normal distribution for wells, 230 (left) and 231 (right)

The aperture distribution parameters, i.e. sample size, mean, standard deviation, maximum, and minimum values for each well are listed in Table 4-1. It should be noted that aperture values are in terms of inches.

Table 4-1: Aperture distribution parameters for each well

Well #	Samp. S.	Mean	Std Dev.	Max.	Min.
72	1275	0.10	0.03	0.24	0.03
137	596	0.09	0.03	0.20	0.04
230	911	0.10	0.03	0.22	0.04
231	853	0.10	0.03	0.26	0.04

On FracMan7, storativity and transmissivity can be correlated to size, trend, plunge, aspect ratio, fracture radius, fracture area, and aperture. Rutqvist et al. [21] provided two equations that correlate aperture to transmissivity and storativity:

$$S = \rho g\left(\frac{A\alpha}{\sigma_n^2} + C_f b\right) \quad (4\text{-}1)$$

$$T = \frac{\rho g}{12\mu}\left(\frac{Af}{\sigma_n} + b\right)^3 \quad (4\text{-}2)$$

In equations above, ‘S’ and ‘T’ are storativity and transmissivity, respectively. ‘b’ is fracture aperture, ‘ρ’ is density, ‘g’ is gravitational acceleration, μ is viscosity, ‘A’ is Goodman’s joint parameter, ‘α’ is Biot’s effective stress constant, ‘σ_n’ is normal stress value, ‘f’ is the fracture factor, and ‘C_f’ is fluid compressibility.

$\left(\frac{A\alpha}{\sigma_n^2}\right), \left(\frac{Af}{\sigma_n}\right)$ Expressions are effective when the reservoir is shallow at which normal stress is relatively small. However, it was discussed earlier that the reservoir section

of Field X is sufficiently deep; therefore, it can be expected that a large normal stress amount exists and the expressions have negligible influence on storativity and transmissivity so that they can be ignored from the equations.

4.1.6 Forward modeling and calibration process

FracMan7 performs a flow calculation using the Galerkin [28] finite element method, which subdivides fractures into smaller triangular elements. For each well under investigation, simulation of fluid flow through fracture network was used to compare each well production test. The pressure change of the simulated build-up was matched to the actual test data (without wellbore storage). An iterative modelling approach was used to converge final description of the fracture network. The reason is unavailability of deterministic measurements for Field X. The fracture parameters except aperture were considered as static tuning structures and used to constraint the actual geometry of the investigated region in an iterative method using a number of steps:

1) Match the actual production test data with a FracMan7 dynamic simulator by adjusting the dynamic tuning parameters, (aperture distribution).
2) If a satisfactory match was not achieved, construct a new DFN model by changing the fracture parameters.
3) Repeat the matching process from the first step.

This step-by-step approach produced a final DFN model whose dynamic response matched closely the actual test data.

4.1.7 Upscaling fracture properties

FracMan7 performs a number of analyses on grids to upscale fracture network properties to grid properties which is appropriate to export to dual-continuum reservoir simulators. FracMan7 applies two kinds of fracture K analysis to characterize fracture system in order to check the scale dependence of the fracture system geometry and upscale the permeability properties: Block K and Oda. Both are used to compute the hydraulic connectivity, or K, of fracture sets contained within a grid by dividing the sets among the grid's set. We applied Oda tensor approach to obtain the hydraulic connectivity properties of fractures. The major

advantage of this approach is that it can obtain EPM properties for grid cells based directly on the geometry and the fractures within those cells. Oda analysis embarks to calculate permeability tensors in three dimensions and all directions for each cell of a given grid. The procedure of the analysis started with projection of the area of fractures in the cell onto a plane parallel to direction of flow. The projected area of a fracture is determined by cross-product of fracture pole and direction of flow multiplied by total area of the fracture. Subsequently, it is multiplied by the transmissivity of fracture in that direction. The results are then added up and divided by the height of the grid being analysed, along the axis parallel to direction of flow. Finally, the fine permeability grids are upscaled to other dual-continuum reservoir simulators. The generated DFN models for each well are illustrated based on their drainage boundaries and assumptions in Figures 4-4 through 4-7.

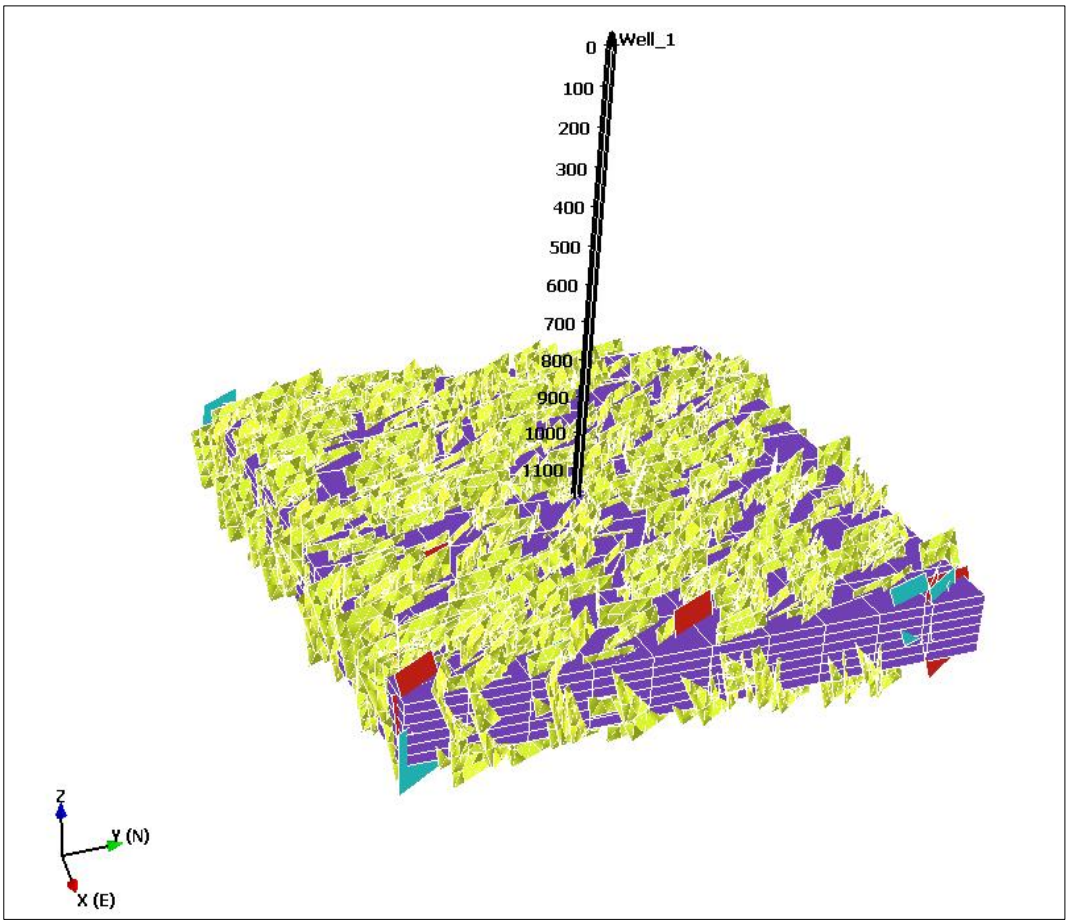

DFN Model Color Scale			
	Grid Block		Fracture Set 1 (Not Meshed) created based on Enhanced Baecher Approach
	Fracture Set 2 (Not Meshed) created based on Enhanced Baecher Approach		Triangular Finite Element Meshes on Connected Fracture Sets for Flow Simulation

Figure 4-4: DFN Model, Well 72

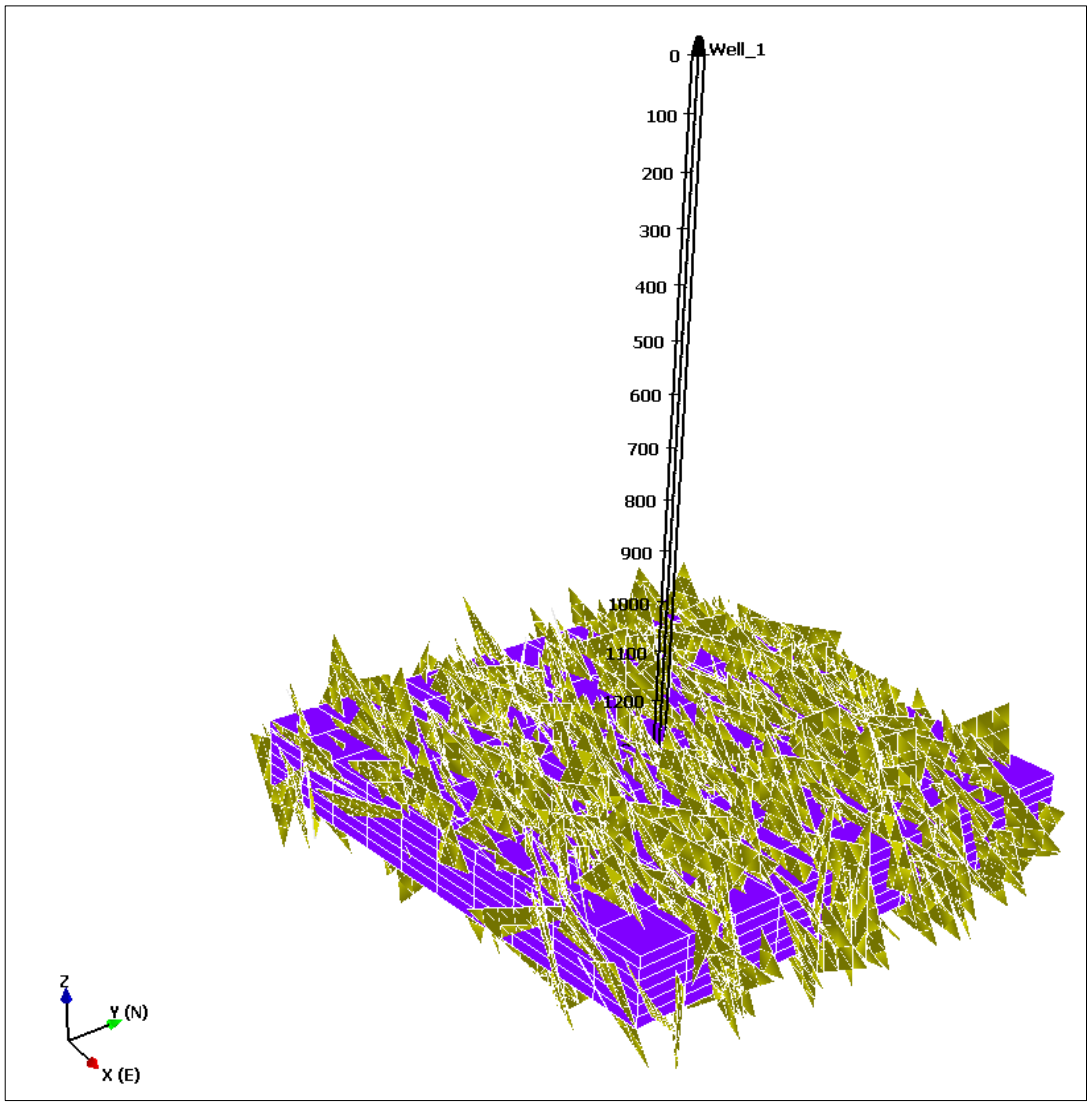

DFN Model Color Scale			
	Grid Block		Fracture Set 1 (Not Meshed) created based on Enhanced Baecher Approach
	Fracture Set 2 (Not Meshed) created based on Enhanced Baecher Approach		Triangular Finite Element Meshes on Connected Fracture Sets for Flow Simulation

Figure 4-5: DFN Model, Well 137

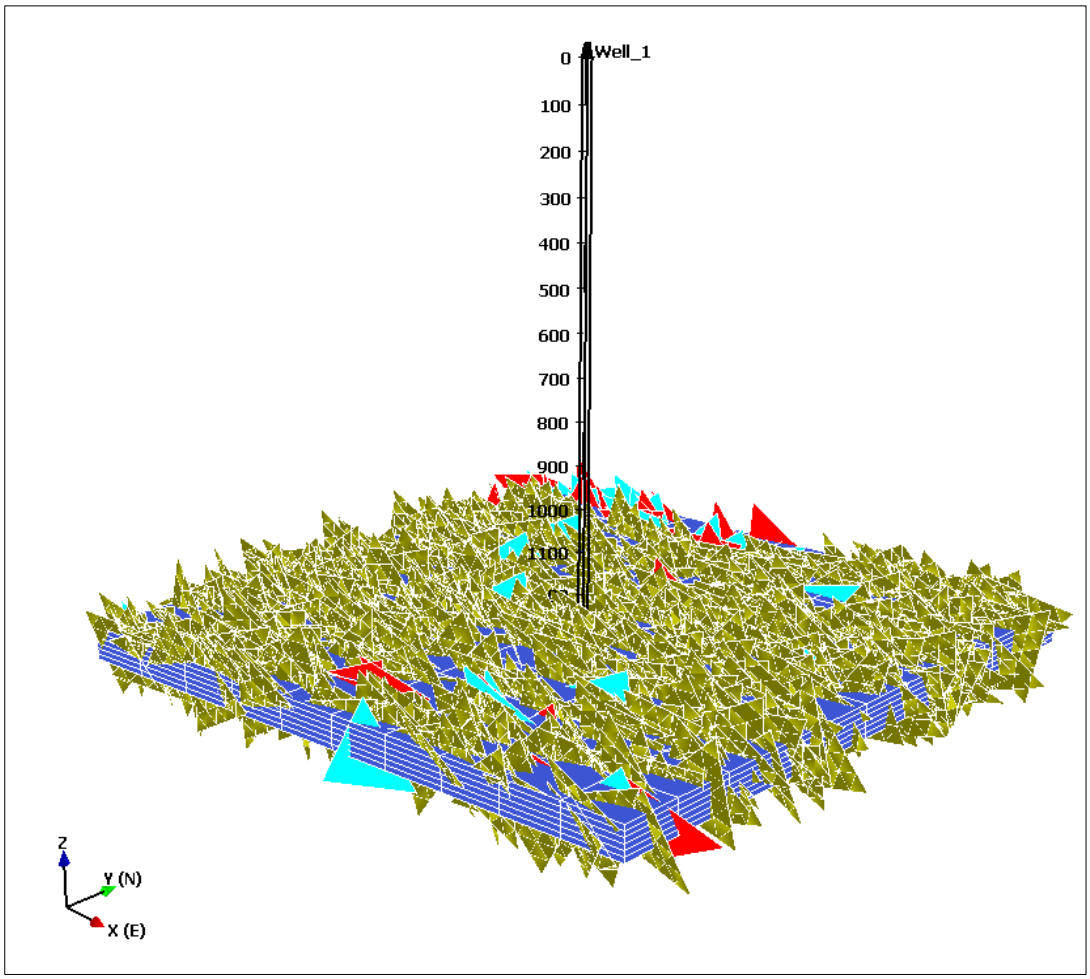

DFN Model Color Scale			
	Grid Block		Fracture Set 1 (Not Meshed) created based on Enhanced Baecher Approach
	Fracture Set 2 (Not Meshed) created based on Enhanced Baecher Approach		Triangular Finite Element Meshes on Connected Fracture Sets for Flow Simulation

Figure 4-6: DFN Model, Well 230

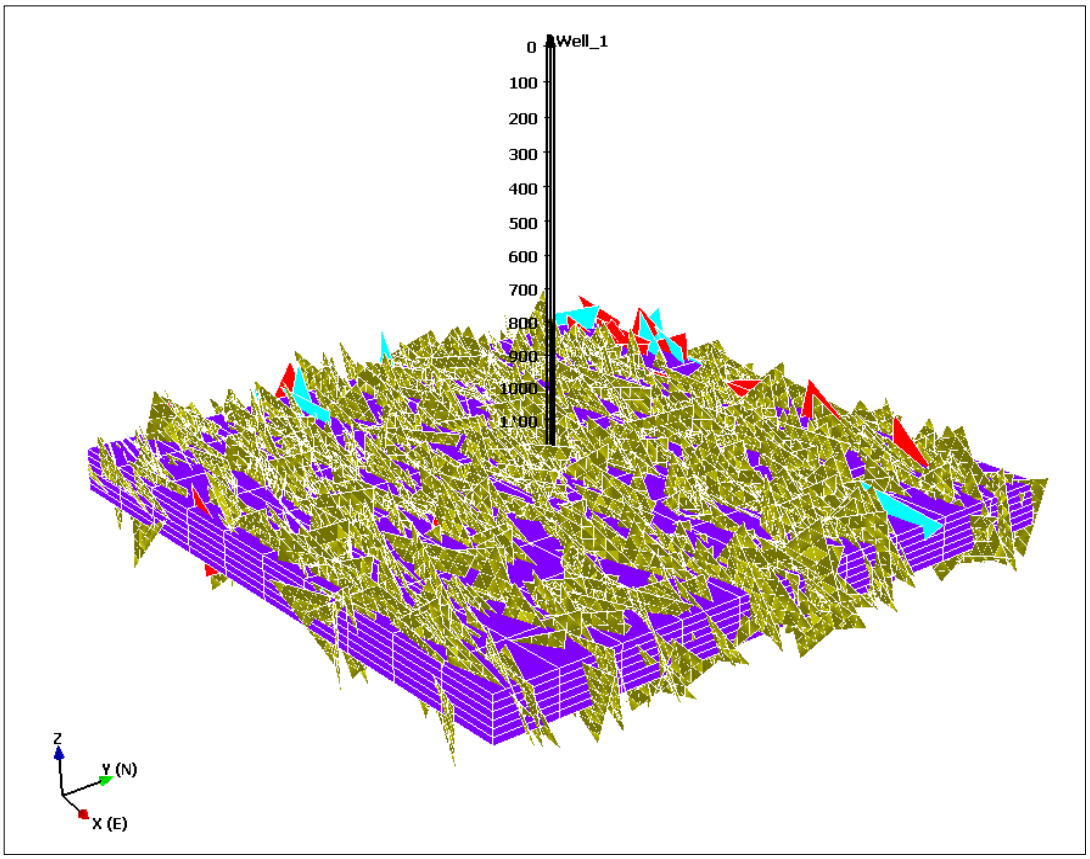

DFN Model Color Scale			
	Grid Block		Fracture Set 1 (Not Meshed) created based on Enhanced Baecher Approach
	Fracture Set 2 (Not Meshed) created based on Enhanced Baecher Approach		Triangular Finite Element Meshes on Connected Fracture Sets for Flow Simulation

Figure 4-7: DFN Model, Well 231

4.2 Generating Dual-Continuum Reservoir Model

In this section, the dual-continuum reservoir model for gel injection simulation based on single cartesian well approach is generated. For this purpose, CMG STARS, a full featured advanced processes reservoir simulator, is used. The simulator governs the fluid and heat flow in naturally fractured reservoirs. The reservoir is discretized into two collected elements. These elements acts like two sets of grid blocks located in the same space. Matrix blocks are one of the continua which are separated spatially by fractures, another continuum. The schematic view of the fractured reservoir model on the simulator is depicted in Figure 4-8.

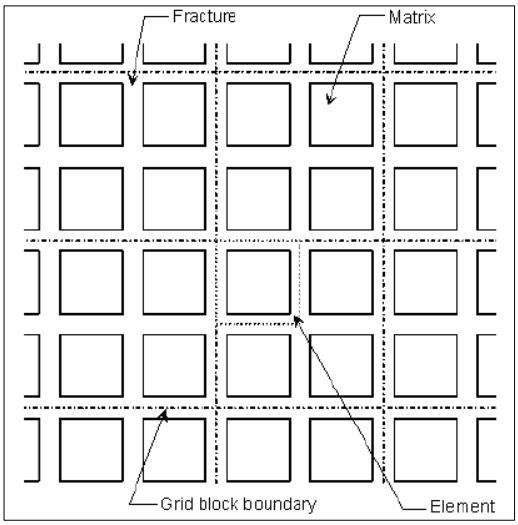

Figure 4-8: Fractured Reservoir Grid Model on CMG Simulator, [39]

4.2.1 Dual-porosity models

One of the most important assumptions that we made during the Field X fracture network modeling is consideration of negligible permeability for matrix continua throughout the reservoir. Field X reservoir is heavily faulted and folded; therefore, it is expected that it contains highly fractured reservoir where according to Kazemi et al. [40] assumption of complete matrix discontinuity is valid. Dual porosity models assume that the fracture network is the primary continuum for the fluid flow. The low permeability, and high storativity matrix is considered to act like a source or sink to the fracture, which is appropriate for highly fractured reservoirs, [41].

4.2.2 Dual-porosity model generation

CMG STARS, utilizes Gilman-Kazemi approach for modeling of dual-porosity system. This model describes stable, flexible, fully implicit, finite-difference simulator in heterogeneous, dual-porosity reservoirs. Flow rates and wellbore pressures are solved at the same time for the fracture and matrix fluid saturations and pressures, [42]. This model allows one distinct value for matrix and fracture's porosity and permeability per grid block, where matrix is connected to the fracture in the same grid block. Fracture porosities and permeabilities (in all directions) are connected to the neighboring fracture porosities and permeabilities in a usual manner. This approach is highly appropriate to our model, since using DFN

simulator the fracture porosities and permeabilities per grid block is already determined.

4.2.3 Flow equations

A numerical method that utilizes for two-phase (Oil/Aqueous) flow according to an extension form of Warren-Root model to multiphase flow is used. Fully implicit Newton-Raphson numerical method is run on CMG STARS. According to the software User's Guide, in many cases a small number of grid blocks are needed to be solved fully implicitly and most blocks are solved by the explicit numerical method, [39]. The partial derivative equation considers gravity, capillary, and viscous forces between matrix and fracture. Polymer gel injection is also simulated in Field X reservoir model; therefore, an additional partial derivative equation to describe chemical flow in fracture and matrix is also considered. The assumption which considers the fractures as the only pathway into the wellbore and the path of fluid flow from one grid to another governs throughout the model. The partial derivative equation according to five-point discretization finite-difference expansion results for given node in each grid center, and also for each i-j, i-k, and j-k planes is created, separately. Each node is dependant only on the unknowns of that node and immediately surrounding nodes. Bottom-hole pressure for each well where the well is completed is solved using fully implicit methods in STARS. Moreover, for the situations of which a well is completed in more than one layer, bottom-hole pressure is solved using fully coupled manner, i.e. the layers are discretized and solved simultaneously.

4.2.4 Initial and boundary conditions

Specified initial and boundary conditions to solve finite-difference equations for Field X are as follows. For the time zero, initial condition is based on initial water saturation data, oil/water contact data, and fluid pressure gradients. At the time zero the initialization confirms the whole system is at gravity/capillary equilibrium. For the times greater than zero, the boundary conditions for the wellbore liquid rate are the constraint and set to be constant. For reservoir outer boundaries, constant pressure-gradient is considered.

4.2.5 Fluid component and its properties

An important aspect of gel injection processes is the interaction between chemical components. In the case of Field X, two aqueous based additives (polymer and crosslinking agent) are injected into oil containing reservoir to block preferential water pathways by reacting to form a pure blocking gel. The method of component preparation for fluid data is given in the subsequent table:

Table 4-2: Fluid components and phases for gel system, [39]

COMPONENT	PHASE		
	Aqueous	Oleic	Adsorbed
Water	X		
Polymer	X		X
Cross-linker	X		
Gel	X		X
Oil		X	

The applied gel for Field X is chromium(III) carboxylate polyacrylamide gel. Chromium(III) chloride is crosslinking agent and the polymer is hydrolyzed polyacrylamide with molecular weight of 8 to 13 MMamu and hydrolysis from 8 – 15%. In this study, cross-linking agent is the synthesis of ion-exchange resins and stimuli-responsive hydrogels made from polymer molecules containing polar groups. As polyelectrolytes hydrogels are characteristically water soluble, when cross-links are added to long rubber molecules, flexibility decreases, hardness increases, and the melting point increase as well.

4.2.6 Rock-fluid data

In this subsection, the relationship between rock and fluid is taken into consideration. The relative permeability and component adsorption of Field X is defined for CMG STARS. The relative permeability data is generated using correlation of relative permeability to reservoir fluid saturation data of the field. The gel adsorption property, which determines the rate of propagation of added gel and interaction of it with rock matrix, is fixed according to default settings of the software.

CHAPTER 5

FIELD DATA ANALYSIS AND THE RESULTS

5.1 Analysis of the Field

The tectonic environment plays an essential role in the generation of fractures in the reservoir. Understanding the tectonic features of the hydrocarbon field under investigation is crucial in fracture discretization. Field X is one of the major oilfields of Turkey which is geographically located in southeastern Turkey. Figure 5-1 illustrates its heavily folded, faulted and fractured anticline structure of producing formation. The field under study is an elongated, strongly faulted NW-SE trending double anticline which gently dips toward north. Two dominant fault sets striking WNW-ESE are observed. Four minor fault sets oriented in NW-SE and WNW-ESE are also present. According to Sener and Bakiler [31], most of the present pore volume in carbonates of main producing zone is created by chalkification, courser recrystallization and concurrent leaching processes. Fracturing, resulting from tectonic events, is another parameter affecting the carbonate rocks of Field X, [31].

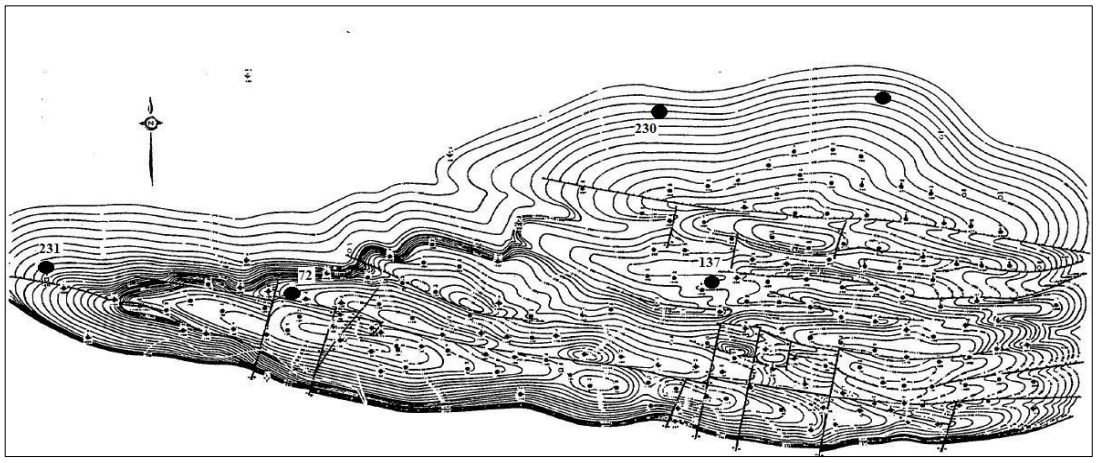

Figure 5-1: Structural contour map and gel treatment wells of field X, [31]

As it was mentioned before, four wells are subject to gel injection simulation. In this study we provide single well fracture network modeling and dual porosity reservoir modeling for history matching analysis. Well based data offered from Field X is listed in Table 5-1. The reservoir contains heavy oil of about 17 API degrees, with negligible gas oil ratio. Viscosity is about 30 cp at bubble point pressure, and reservoir temperature is 140 degrees F, the average reservoir depth is 3900 ft, initial reservoir pressure is 1300 psia, and the connate water saturation is 15%. The total compressibility of the reservoir is $9.77(10^{-6})$ 1/psi, and oil formation volume factor at bubble point pressure of 325 psi is 1.061. Sener and Bakiler [31] indicated that the presence of strong aquifer and vertical fractures maintain reservoir pressure to remain nearly constant throughout the reservoir. Similarly, they noted that vertically directed fracture minimize the lateral fluid flow, and therefore single well modeling approach can be assumed for the case of Field X.

Table 5-1: Well-based field data

	Well 72	Well 137	Well 230	Well 231
Porosity (%)	14	12	15	11
Permeability (mD)	204	116	65	1920
Gel Interval (m)	1222-1229	1410-1473	1315-1327	1342-1374
DST Interval (m)	1220-1226	1406-1430	1312-1332	1348-1359.5
Pressure from DST (Psia)	880	1318	1230	1077
Pressure at -200 m datum (Psia)	1081	1187	1120	1094
Reservoir Pressure after year 2013 (Psia)	1090	1126	1115	1100

The gel injection treatment for wells of Field X is conducted in three or four stages. In each stage the concentration of polymer and cross-linker has changed to reach the optimum viscosity and appropriate set-up inside the fractures, [43]. Stages were separated based on the concentration of injected gel. In the first stage the pre-gel treatment was implemented. Small volume of lowest concentration gel was applied in this stage. In the further stages, a more durable and concentrated gel in order to settle and fix in the fractures was injected. In the last stage, smaller volume of the

most concentrated gel was applied to set around the wellbore. Since the greatest pressure drop occurs around the wellbore the final stage gel should be selected so that it tolerates the pressure drop. The previous gel treatment operation data for each well under investigation are given in Figures 5-2 through 5-4. The gel injection operation information for well 137 is not available. Well 230 was treated in four stages and the major volume of injection was implemented in second and third stages.

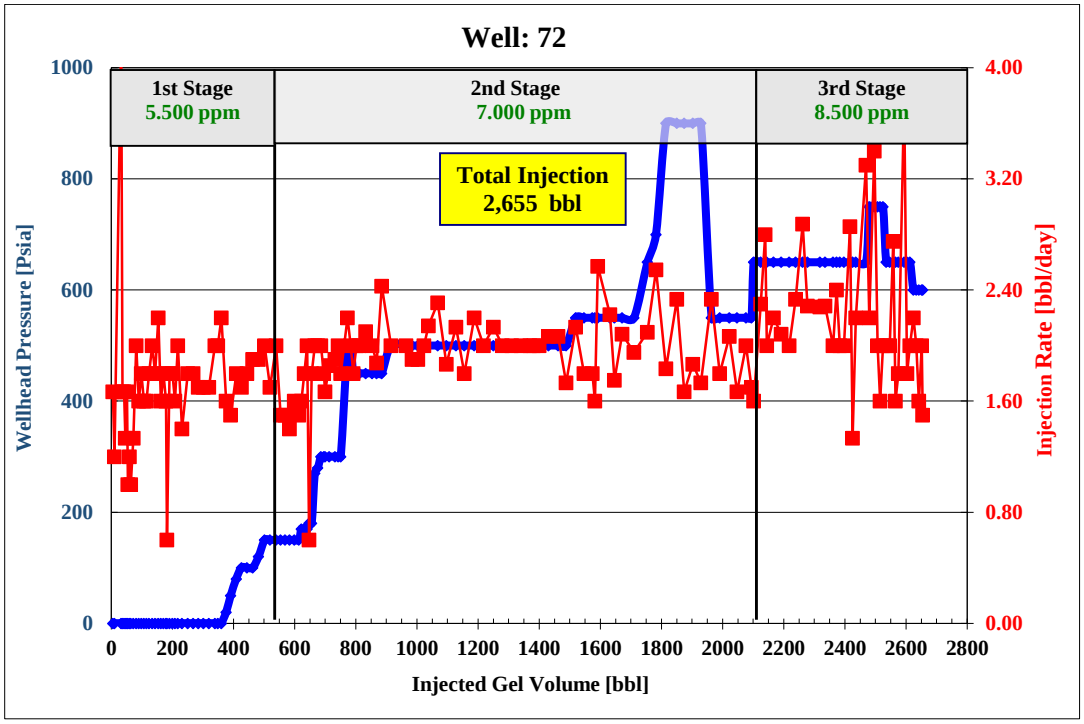

Figure 5-2: Well 72 gel injection operation

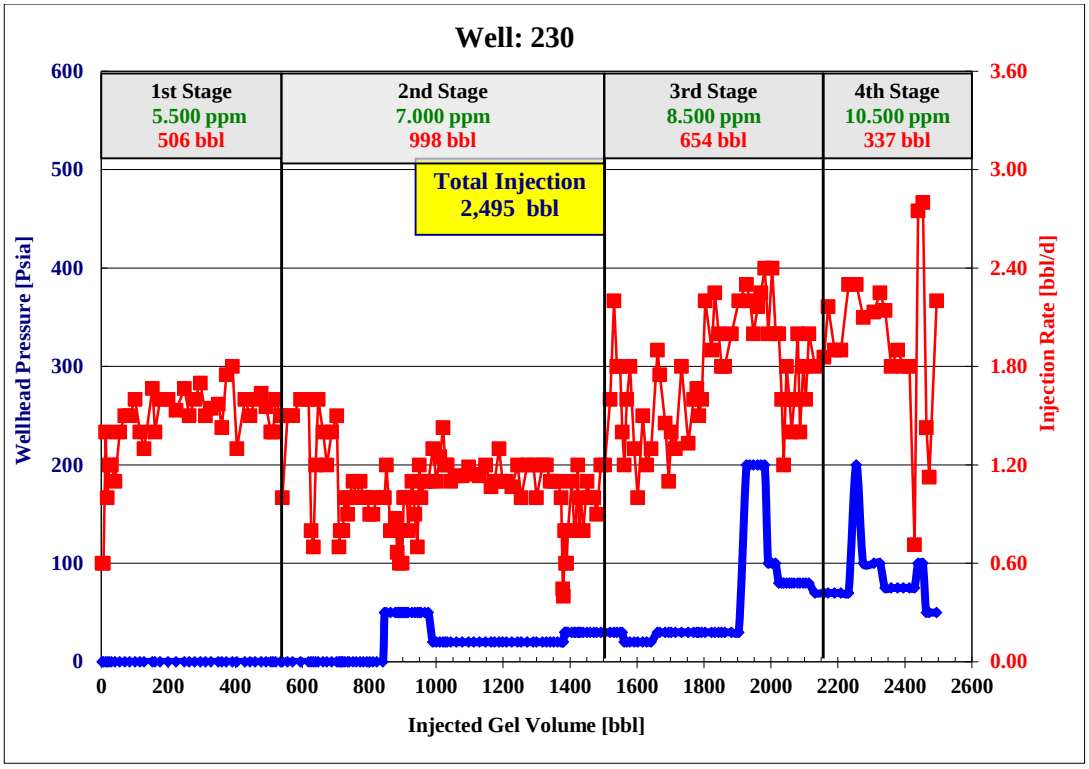

Figure 5-3: Well 230 gel injection operation

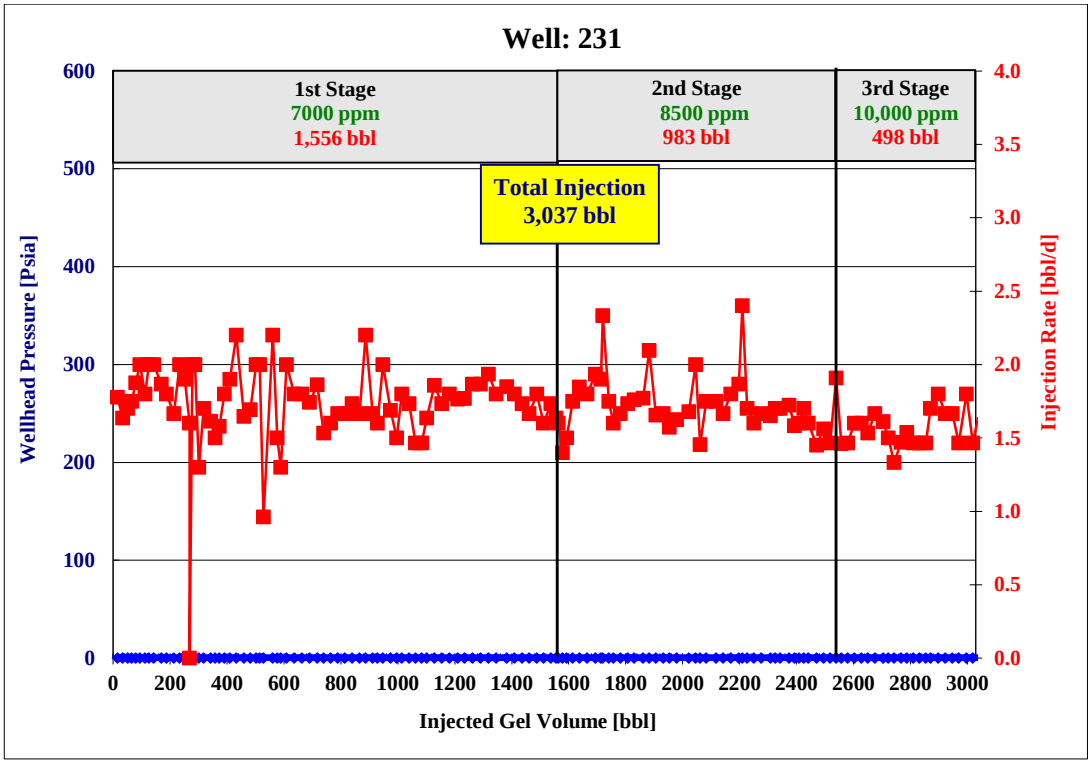

Figure 5-4: Well 231 gel injection operation

5.2 Determination of drainage radius

We are going to model each well individually; therefore, determination of the drainage radius of each well is needed to be determined. Since all of these wells have been producing for several years it is assumed that they are producing under semi-steady state condition such that each well will drain from within its own no-flow boundary without any effect of the other wells, [1]. Therefore, under the assumption of constant pressure decline rate throughout the reservoir Matthews et al. (1954) suggested Formula 5-1 to calculate the drainage radius of well:

$$A = \frac{0.23396\ q\ t}{C_t \varphi\ h\ (P_i - \overline{P_r})} \qquad (5\text{-}1)$$

Where,

A = Drainage radius (ft^2)
q = Flow rate (bbl/d)
t = Elapse time from the end of transient flow regime (hrs)
C_t = Compressibility (1/psi)
φ = Porosity (frac)
h = Reservoir Thickness (ft)
P_i = Initial Reservoir Pressure (Psia)
P_r = Volumetric Average reservoir pressure (Psia)

The volumetric average reservoir pressure can be determined according to:

$$\overline{P_r} = \frac{\sum(\overline{P_{ri}}\ q_i)}{\sum(q_i)} \qquad (5\text{-}2)$$

Where,

P_r = Volumetric average reservoir pressure (Psia)
q_i = Flow rate (bbl/d)
$\overline{P_{ri}}$ = Average pressure within i-th drainage volume (Psia)

The resultant table for approximated drainage area and drainage radius of each well is listed in Table 5-2.

Table 5-2: Drainage area and drainage radius of each well

	A (ft^2)	r (m)
Well 72	20924794	786
Well 137	9588309	532
Well 230	20362759	776
Well 231	34067003	1003

5.3 DFN dynamic simulation

Based on the stochastic distribution of each parameters according to the methodology discussed earlier DFN model is produced. As dynamic analysis, well test simulation is implemented on fracture sets to justify the veracious of applied geometrical parameters. The well test data provided from the field are not so precise. These data are based on production of the wells in the period of several years. Therefore, we compare the simulation results with well test results at first point and end point of simulated well test results. At each step, if pressure simulation did not match with real test pressure, first of all dynamic tuning parameters are adjusted. If the appropriate match has not been reached the DFN model is implemented again by tuning static geometrical parameters. The final well test simulation bottom-hole pressure curve vs. time is revealed in Figures 5-5 through 5-8 for wells 72, 137, 230, and 231, respectively.

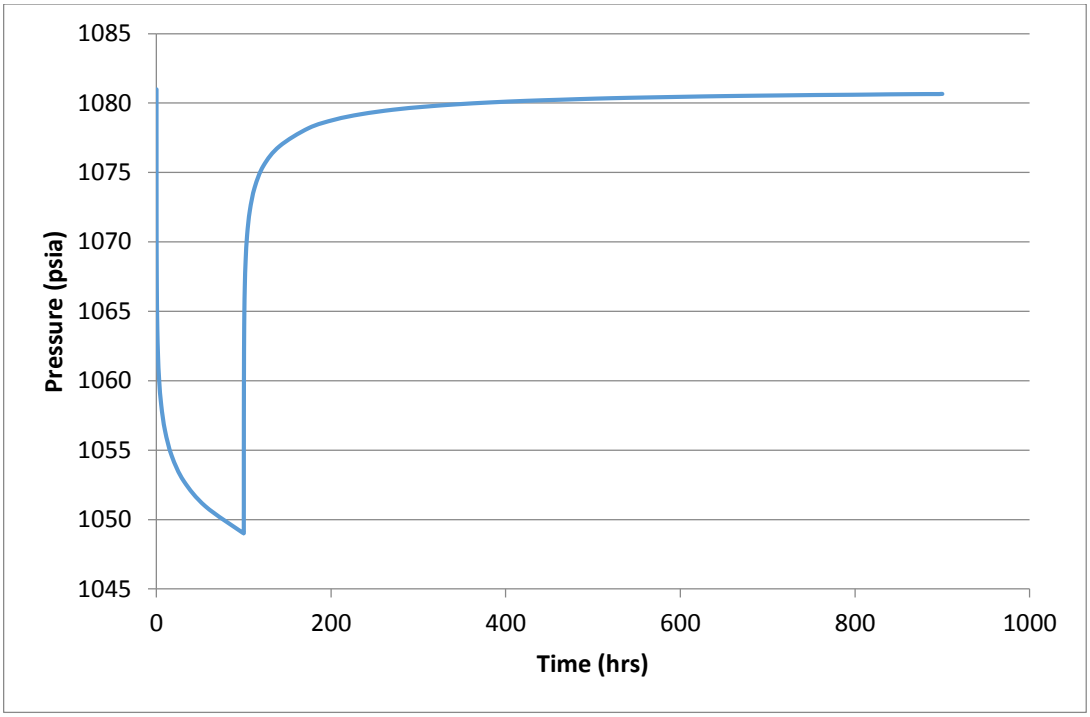

Figure 5-5: Well test simulation - Well 72

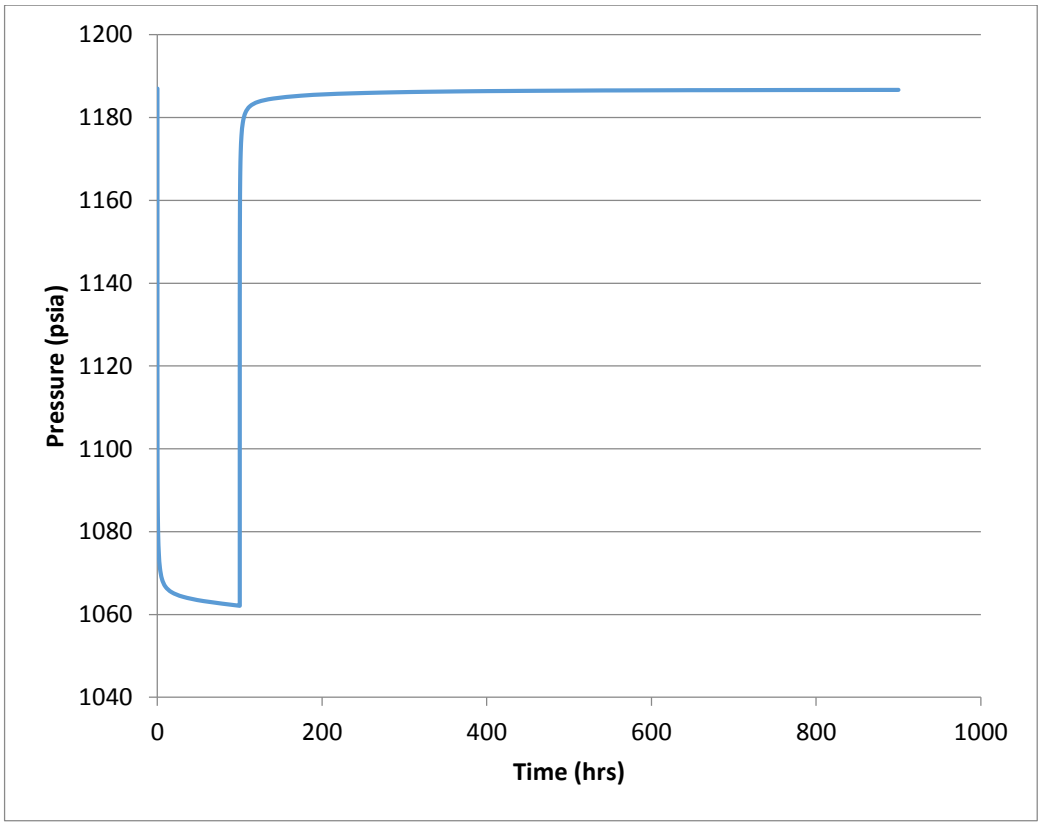

Figure 5-6: Well test simulation - Well 137

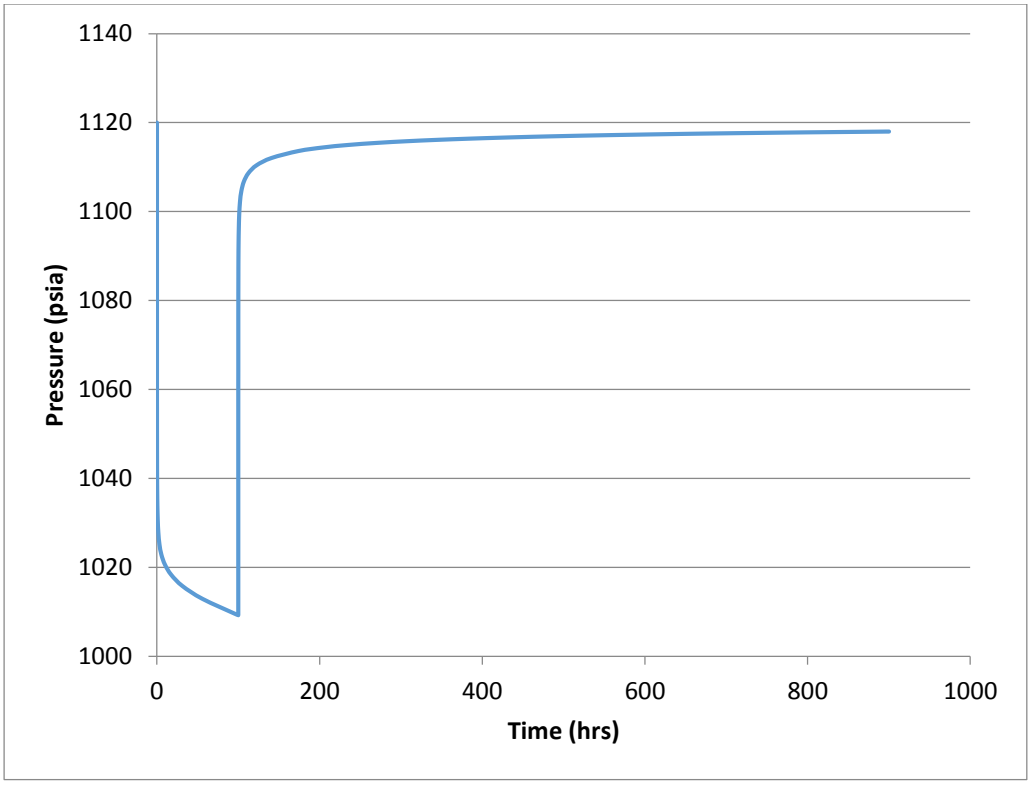

Figure 5-7: Well test simulation - Well 230

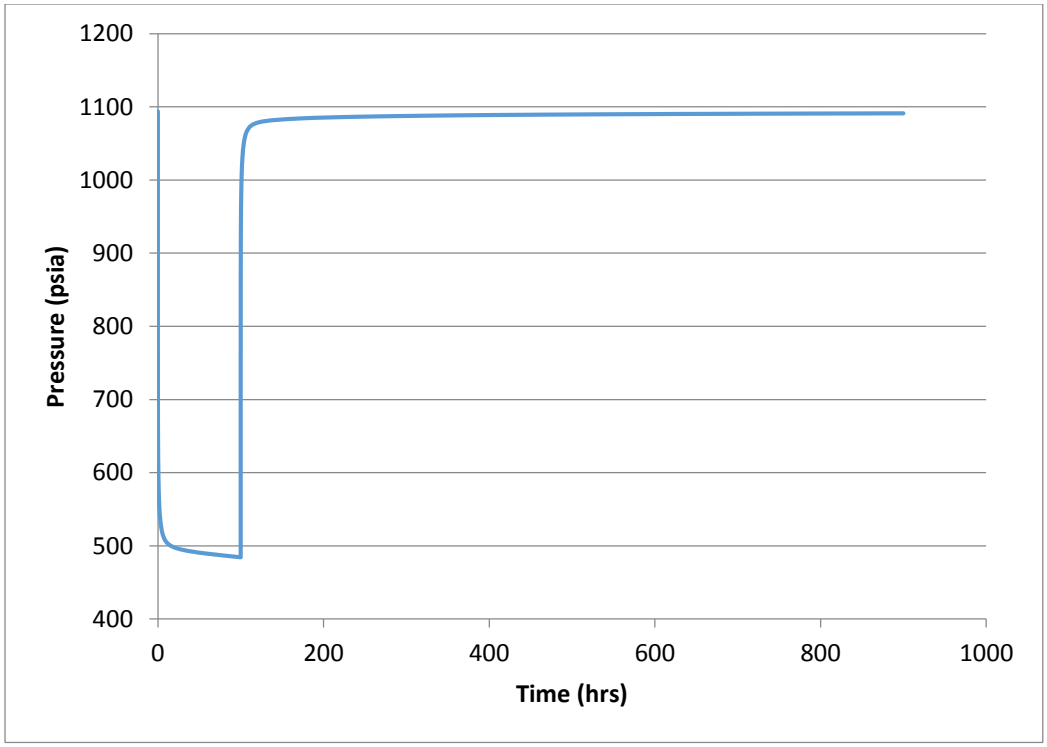

Figure 5-8: Well test simulation - Well 231

In Table 5-3, the well test matching between field pressure results and simulation pressure results are listed:

Table 5-3: Well test pressure table

	Well 72	Well 137	Well 230	Well 231
Initial Pressure (Psia)	1081	1187	1120	1094
Pressure at the beginning of build-up test – Field (Psia)	1052	1062	1050	797
Pressure at the beginning of build-up test – Simulation (Psia)	1049	1079	1009	484
Pressure at the end of build-up test – Field (Psia)	1084	1154	1085	1075
Pressure at the end of build-up test – Simulation (Psia)	1081	1186	1117	1091

To compare simulation test results with real test results, Table 5-4 is provided. In this table, 'absolute relative error' values are obtained at starting and ending points of build-up test.

Table 5-4: Absolute Relative True Error table

	Well 72	Well 137	Well 230	Well 231
Abs. True Error at Starting point, %	0.3	1.6	3.9	39
Abs. True Error at Ending point, %	0.3	2.7	2.9	1.4

The schematic view of generated DFN model for each well is depicted on figures 4-4 through 4-7. During calibration process of DFN model based on the available parameters two fracture sets were generated for all wells. The selected fracture shape is rectangular for well 72, and triangular for the rest of the wells. Some of the fractures are not connected to the other fractures and wellbore; hence, they do not contribute to fluid flow simulation. FracMan7 did not generate finite element meshes on these fractures, and they left in original colors assigned by FracMan7. Except fracture sets of well 137 other wells' fracture sets have some fractures with no contribution in fluid transport.

5.4 Upscaled fracture properties

In this section, the upscaled fracture porosity and permeability, which is determined based on Oda's approach, are reported. The fracture porosity and permeability in all directions are listed in Table 5-5 for each well:

Table 5-5: Upscaled fracture properties

	Well 72	Well 137	Well 230	Well 231
Number of grids	600	600	600	600
Max. porosity, %	1.12	1.61	1.11	0.83
Min. porosity, %	0.08	0.09	0.11	0.04
Avg. porosity, %	0.53	0.67	0.54	0.38
Max. permeability in 'i' direction, md	6188	15731	10666	11255
Min. permeability in 'i' direction, md	212	711	672	240
Avg. Permeability I, md	1724	5656	4605	3171
Max. permeability in 'j' direction, md	10133	3673	2780	2105
Min. permeability in 'j' direction, md	582	99	80	33
Avg. Permeability j, md	3802	1108	778	518
Max. permeability in 'k' direction, md	10784	16209	9820	10800
Min. permeability in 'k' direction, md	709	665	638	218
Avg. Permeability k, md	4385	5518	4289	2964

5.5 Dual Porosity Reservoir Model

When DFN fracture properties have been determined and grid-based permeability tensor are generated and fracture porosity has been assigned to each gird, the results are imported to dual porosity reservoir simulator. The single well cartesian reservoir model grid sizes are chosen to be identical to the FracMan7 DFN grids that are generated for reservoir section of each well. The dimensions of the generated model are determined based on the aforementioned drainage area and reservoir thickness of each well. The aim of the dual porosity model is to prepare a history match analysis. In order to create production history data, fluid component properties and relative permeability data are required for creating and solving flow equations.

5.5.1 Properties of fluid

The Field X reservoir contains very low gas oil ratio. Therefore, two phase flow is taken into account. Subsequently, properties of existing oil and water in the reservoir, and the injected polymer gel properties for pre-gel treatment, polymer

treatment, and cross-linking agent application are introduced. Sener and Bakiler [31] mentioned that lower parts of the reservoir contain lower API gravity oil at higher temperature, and conversly for higher parts of the reservoir. Therefore, fluid viscosity varies according to the depth of the reservoir section. In our simulation, we assigned single value for reservoir fluid density, temperature, and viscosity. As a result, during history matching based on given criteria these values were subject to change between the specified ranges. In Table 5-6 the average properties of these components are listed:

Table 5-6: Average properties of reservoir and injected fluids

	Water	Xlinker	Xanthan	Pre-gel	Dead Oil
Phase	Aqueous	Aqueous	Aqueous	Aqueous	Oleic
MW, lb/lbmol	18	206	7500 - 9000	5500 - 7000	639
Density, lb/ft^3	62.4	62.4	62.4	62.4	59
Viscosity, cp	1.0	0.5	0.5	0.5	30

5.5.2 Relative permeability curves

CMG STARS generates relative permeability curves for two-phase flow according to correlations from the literature. The relative permeability curves are generated separately for matrix and fracture. For rock matrix, single oil and water relative permeability curves are generated using irreducible water saturation, residual oil saturation, oil relative permeability at connate water saturation, and water relative permeability at residual oil saturation. For water-wet carbonate reservoir of Field X, Honarpour et al. [44] correlations was used. Equation 5-3 stands for water relative permeability, equation 5-4 is for oil relative permeability. Correlation to matrix porosity and permeability was used for generation of water relative permeability curve. Since oil relative permeability at connate water saturation and water relative permeability at residual oil saturation was not available during history matching, these values were subject to modify.

$$k_{rw} = 0.0020525\,\frac{S_w - S_{wc}}{\varphi^{2.15}} - 0.051371(S_w - S_{wc})\left(\frac{1}{k_a}\right)^{0.43} \quad (5\text{-}3)$$

$$k_{ro} = 1.2624\,\frac{S_o - S_{or}}{1 - S_{or}} * \left(\frac{S_o - S_{or}}{1 - S_{wi} - S_{or}}\right)^2 \quad (5\text{-}4)$$

Where,

S_w = Water Saturation (frac.)
S_{wc}= Critical Water Saturation (frac.)
φ = Porosity (frac)
k_a = Absolute permeability (md)
S_o = Oil Saturation (frac.)
S_{or} = Residual Oil Saturation (frac.)
S_{wi} = Initial Water Saturation (frac.)

Since we assumed very low permeability for matrix and assumed that fractures are mostly contributing to total permeability, we take the absolute permeability for matrix as 2 md throughout the reservoir. Matrix relative permeability to oil and water for each well are revealed in Figures 5-9 and 5-10 reveal under consideration of this assumption.

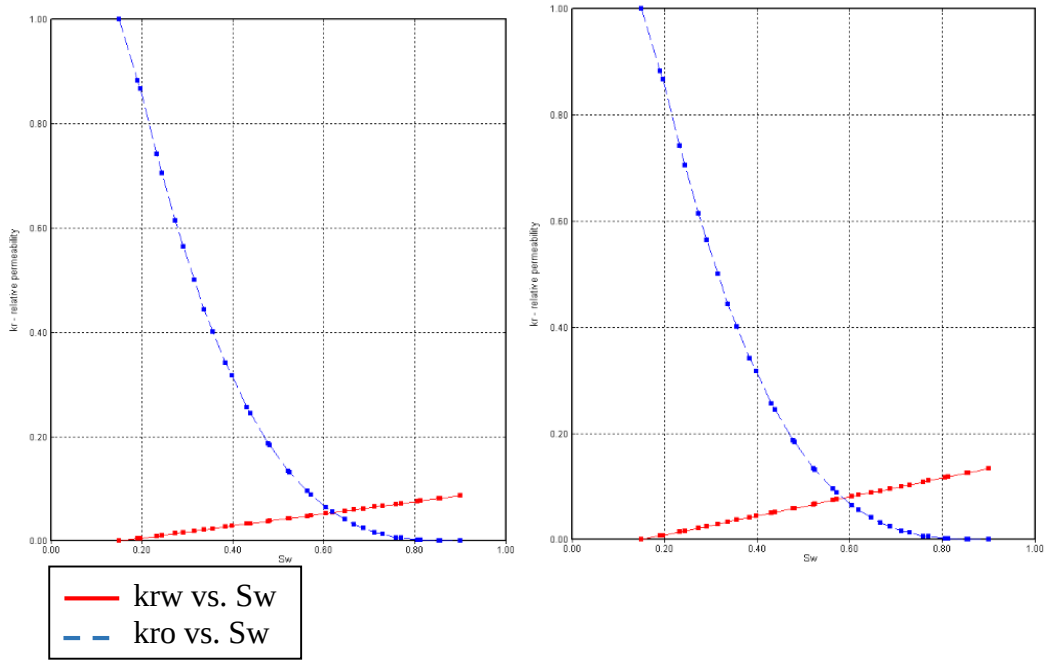

Figure 5-9: Oil (Blue) and water (Red) relative permeability for matrix - Well 72 (Left) & Well 137 (Right)

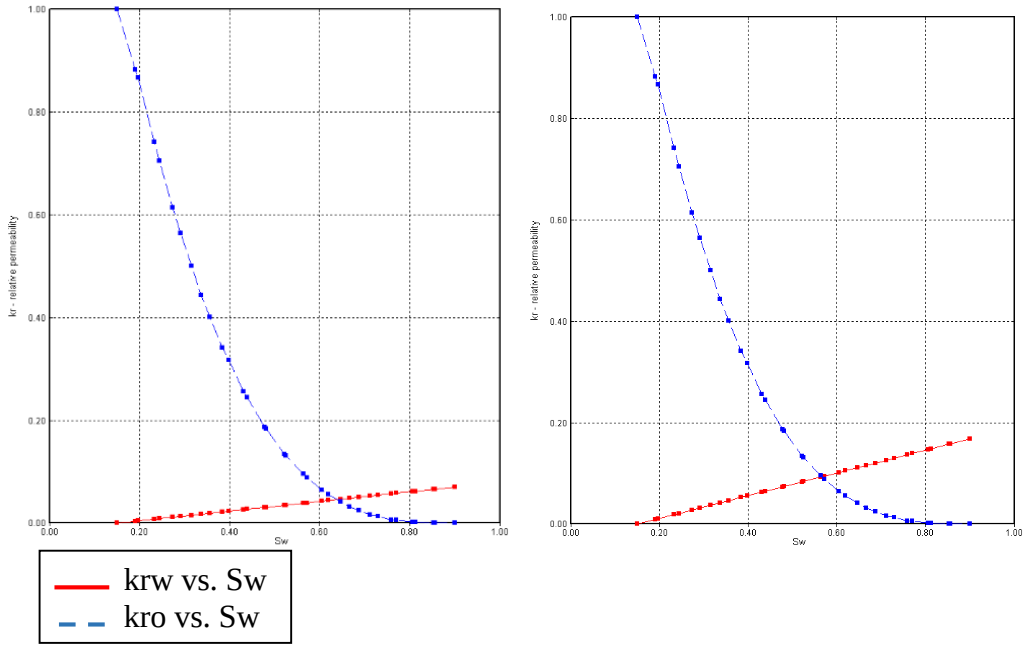

Figure 5-10: Oil (Blue) and water (Red) relative permeability for matrix - Well 230 (Left) & Well 231 (Right)

In STARS Stone's Second model is applied to calculate relative permeability to oil and water for fracture system, [39]. Van Golf-Rakht [45] assumed relative permeability curves as two straight lines with angle of 45 degrees in fractures. In later studies, Akin [46] and Izadi et al. [47] in two different measurements declared that fracture relative permeability should be non-linear function of its corresponding phase saturation. For the case of Field X, we did not have any information about irreducible water and residual oil saturation in fracture. Fatemi et al. [48] assumed these saturations in fractures as zero. Similarly, we considered irreducible water and residual oil saturations to be equal to zero on relative permeability curves. In Figure 5-11 relative permeability for fracture system is provided.

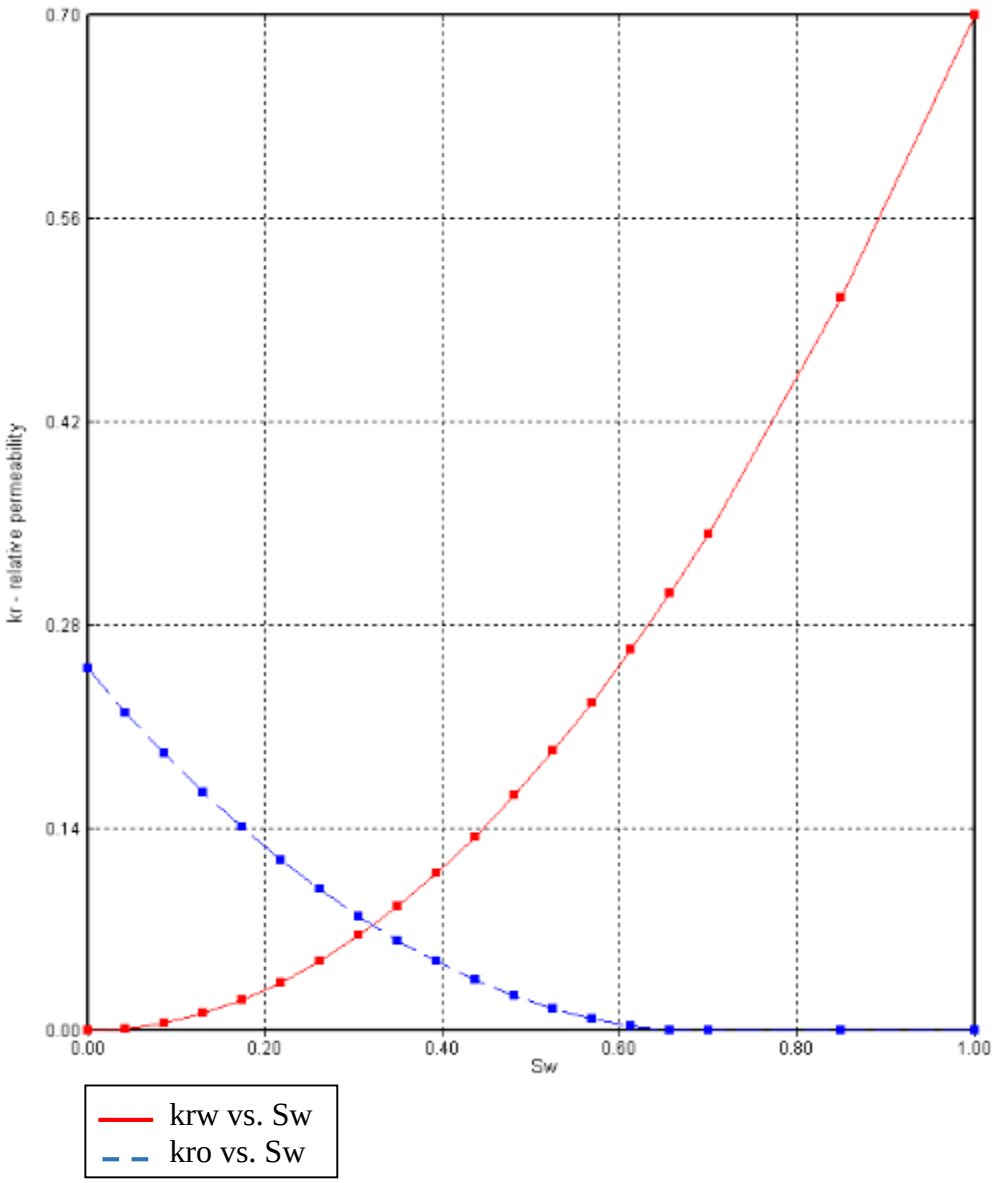

Figure 5-11: Relative permeability for fracture system, oil (blue) & water (red)

5.5.3 Attaining thermal properties of matrix and fracture

Although thermal operators were not used, since STARS is a thermal simulator we applied thermal properties of rock and fractures based on their composition and mineral type according to Table 5-7.

Table 5-7: Thermal properties of reservoir rock and fluid

	Matrix	Fracture
Heat Capacity, Btu/ft^3-F	35	0
Thermal Conductivity, Btu/ft-day-F	37.44	0
Thermal Conductivity of water, Btu/ft-day-F	8.6	8.6
Thermal Conductivity of Oil, Btu/ft-day-F	2.21	2.21

According to STARS user's guide, the heat capacity and thermal conductivity of fractures are zero, [39]. The heat capacity for carbonate and water phase in the system is taken based on default values of CMG STARS. The thermal conductivity of matrix is correlated to graph provided by Robertson, which approximate carbonate conductivity with water in pores measured at temperature of 300°K and pressure of 5MPa, [49]. According to the graph, for average porosity of 14% of the reservoir the value of 2.7 W/mK which is converted to 37.44 Btu/ft-day-F is considered.

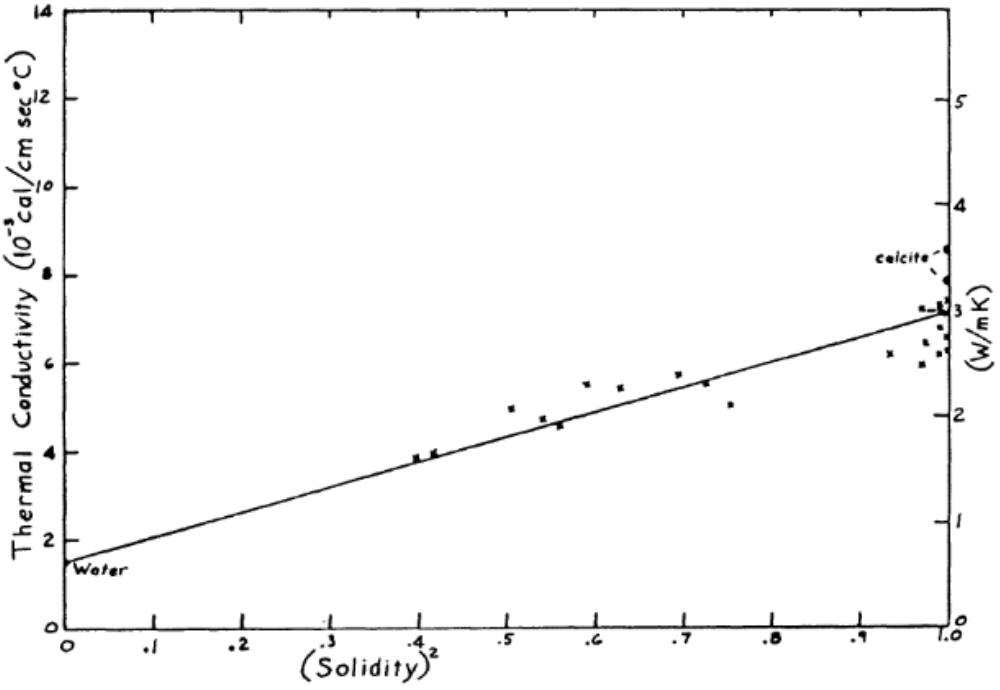

Figure 5-12: Thermal conductivity of carbonate with water in pores, showing the variation of solidity (1 - φ), at 300° K and 5 MPa, [49]

Mansure [50] provided a formula to correlate thermal conductivity of oil from average reservoir pressure and specific gravity of oil:

$$k_o = 1.62 \cdot \frac{1-0.0003(T_{avg}-32°\text{F})}{\gamma_o} \quad (5\text{-}5)$$

Where,

k_o = Thermal conductivity of oil, Btu/ft-hr-F
T_{avg} = Average reservoir temperature, °F
γ_o = Specific gravity of oil

When the reservoir properties data, fluid component data, and relative permeability information is introduced, flow equations based on the previously discussed initial and boundary conditions are generated by CMG STARS. As it was discussed in the previous chapter, for numerical solution of flow equation one of the boundary conditions is wellbore rate, which in the generated model the liquid rate served as constraint.

5.6 History Matching

The history match results of each well are provided in this part. For each well water-cut, oil rate, and liquid rate is compared. Sener and Bakiler [31] separated the reservoir into three different characteristic behaviours. The south and south east of the reservoir were considered as first characteristic behavior section. This section is separated from aquifer by the intervening platformal limestone; the reservoir is structurally deeper in this section; aquifer influx is slow; and wells have high productivity in this part. On the other hand, the north and north east of the reservoir have different characteristics. The aquifer has direct communication with reservoir fluid in this section; the reservoir section is thinner and shallower; aquifer influx is fast; and wells have moderate productivity. According to Sener and Bakiler [31], the rest of the reservoir which comprises most of its region has intermediate characteristics between two aforementioned characteristics. These location based characteristics are the main constraint that we considered during the history matching.

Goodness-of-fit statistical analysis is run to describe how well the results calculated from model fit to field observations. To achieve this, variance of the measurement error is used to construct a weighted sum of squared error. Subsequently, the

reduced chi-squared statistics is utilized by simply dividing it to each data set's degrees of freedom.

$$X_{red}^2 = \frac{1}{\nu} \cdot \sum \frac{(O-E)^2}{\sigma^2} \quad (5\text{-}6)$$

Where,

X_{red}^2 =	Reduced chi-squared statistic
O =	Observed data of Field X
E =	Theoretical data of STARS simulation
σ^2 =	Variance of the observation
ν =	Number of degrees of freedom

As a rule of thumb, if the calculated reduced chi-squared is significantly greater than one, then it is said that the model is purely fit to the observed data. If it is slightly greater than one, it can be indicated that the fit has not fully captured the data. If it is exactly one it can be said that the model results fit the observation, and the fit is in accord with the error variance. If it is less than one, then the model is not fully fit with the observed data.

An iterative approach is considered for obtaining final history matching results. Firstly, a run for water-cut and oil rate matching is conducted with initial reservoir rock, reservoir fluid, injection fluid data and their properties. Secondly, goodness-of-fit statistical analysis besides visual trend are checked for both water rate and oil rate using equation 5-6. Thirdly, the considered fluid properties data and relative permeability curves for matrix and fracture are modified based on available reservoir characteristics data and assumptions. The matching process is continued from the second step until final match is reached.

The history matching results for each well are illustrated in Figures 5-13 through 5-20. In the figures, oil rate and water-cut producing from the wells are revealed. The results of field production history data and CMG STARS reservoir model production data are compared, accordingly. Reduced chi-squared statistical analysis in order to measure the goodness-of-fit for each observed and estimated results is provided for every well.

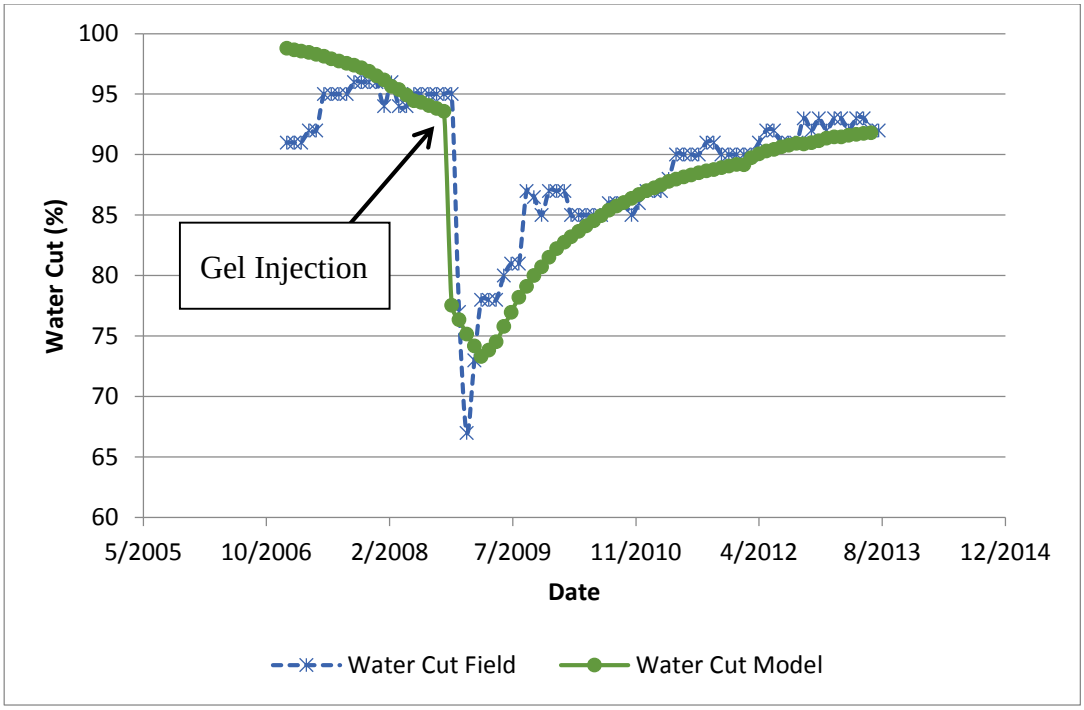

Figure 5-13: Well 72, water cut history matching

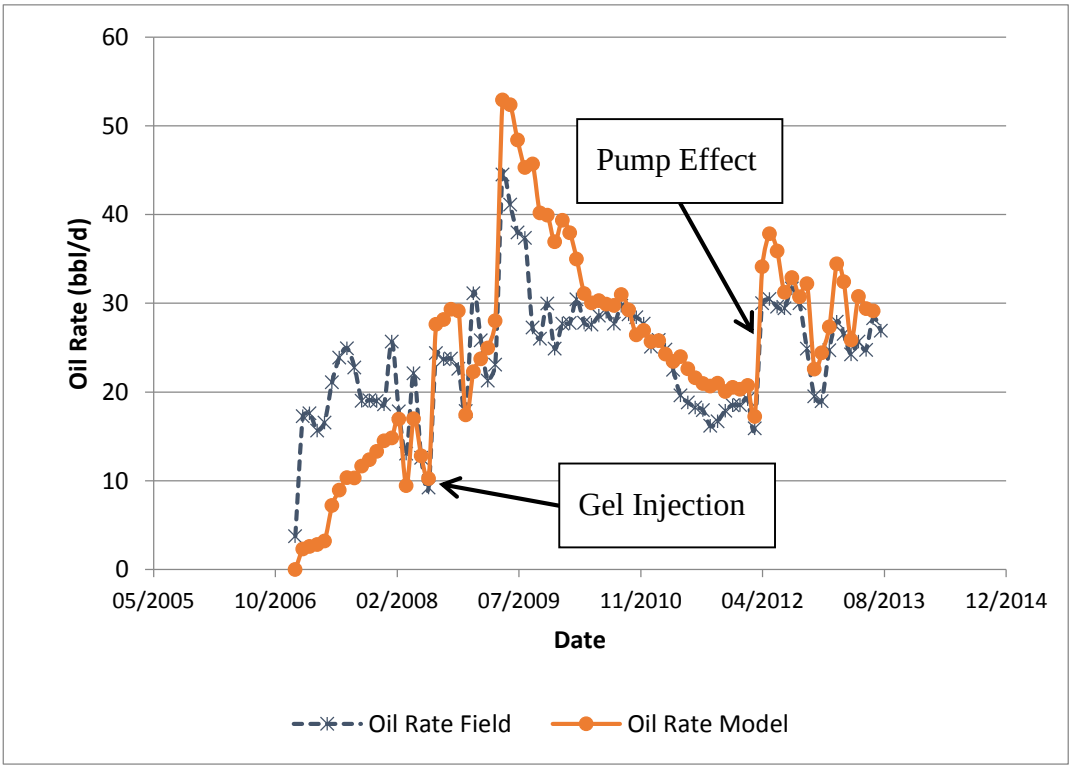

Figure 5-14: Well 72, oil rate history matching

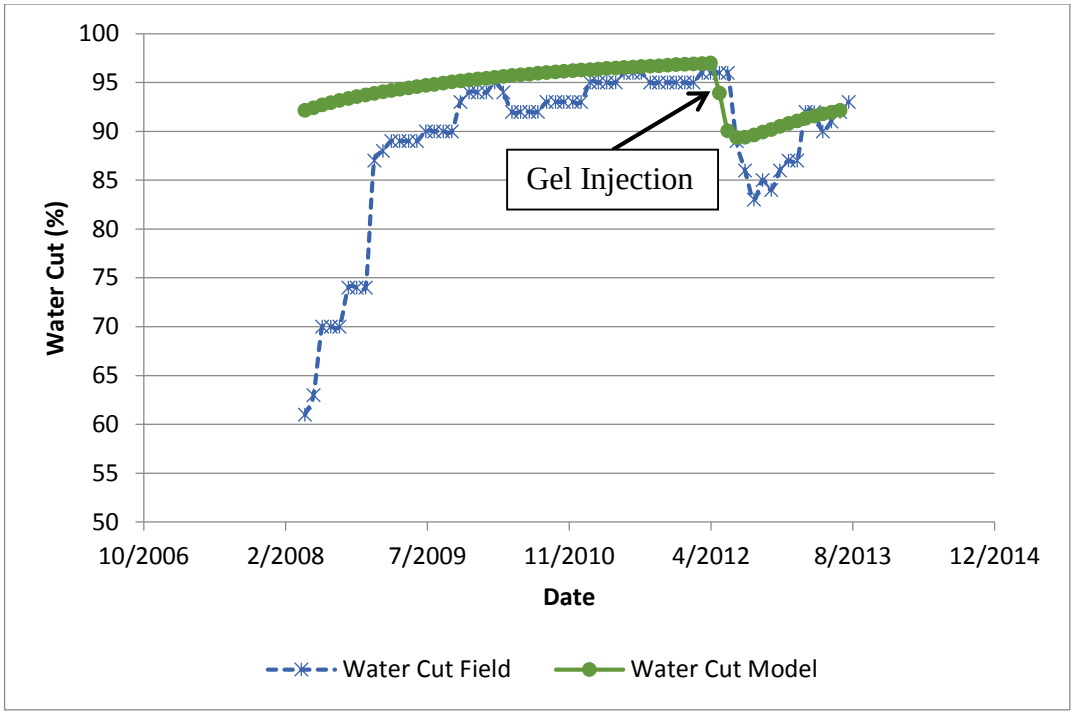

Figure 5-15: Well 137, water cut history matching

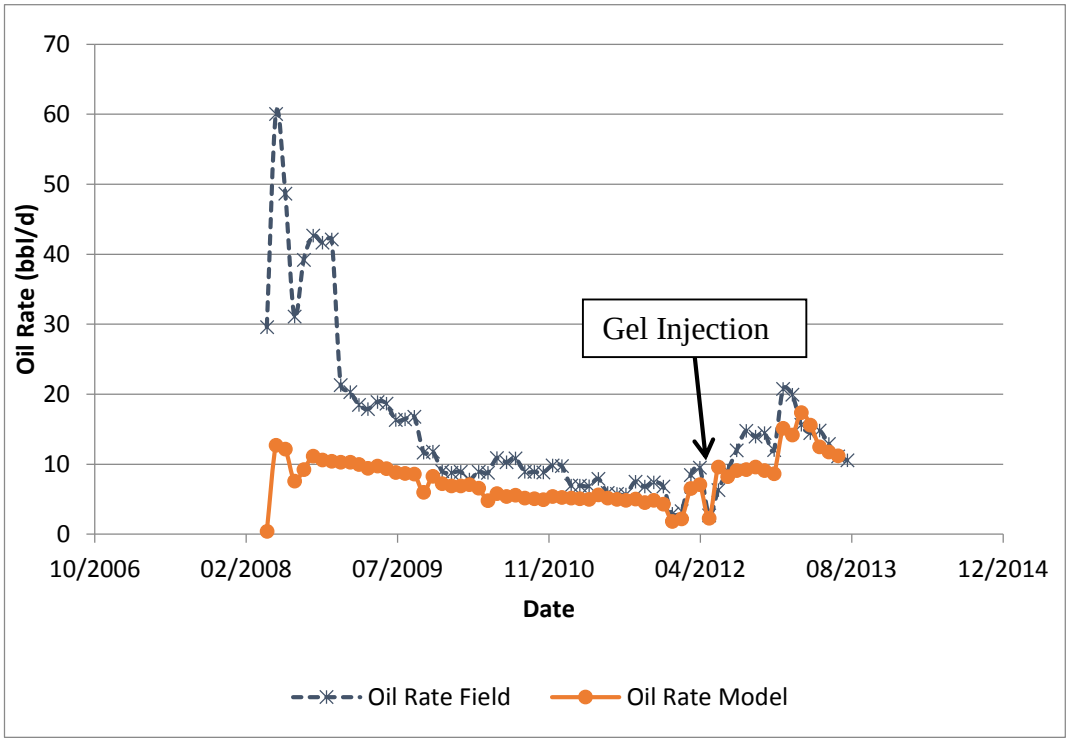

Figure 5-16: Well 137, oil rate history matching

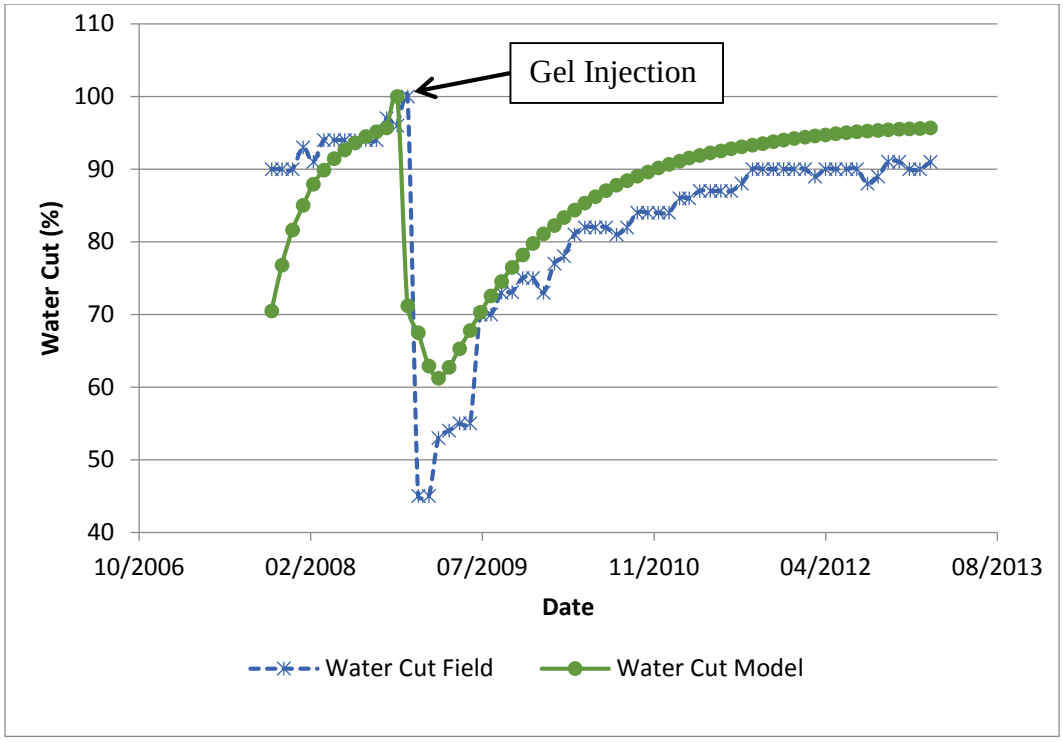

Figure 5-17: Well 230, water cut history

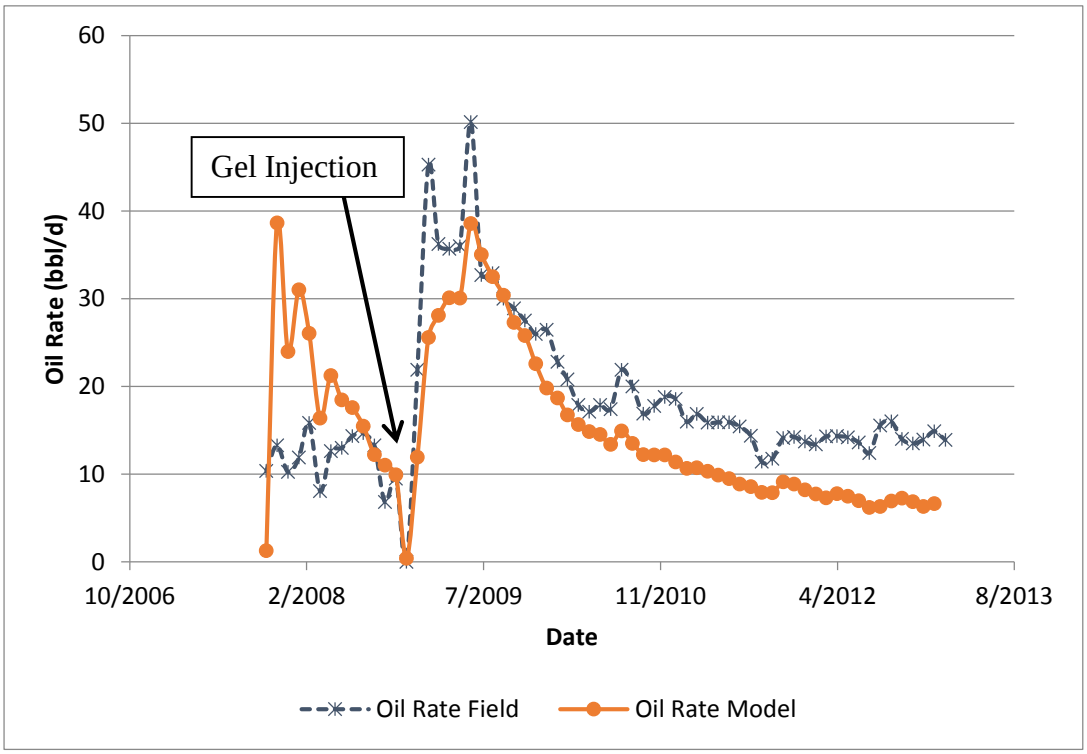

Figure 5-18: Well 230, oil rate history matching

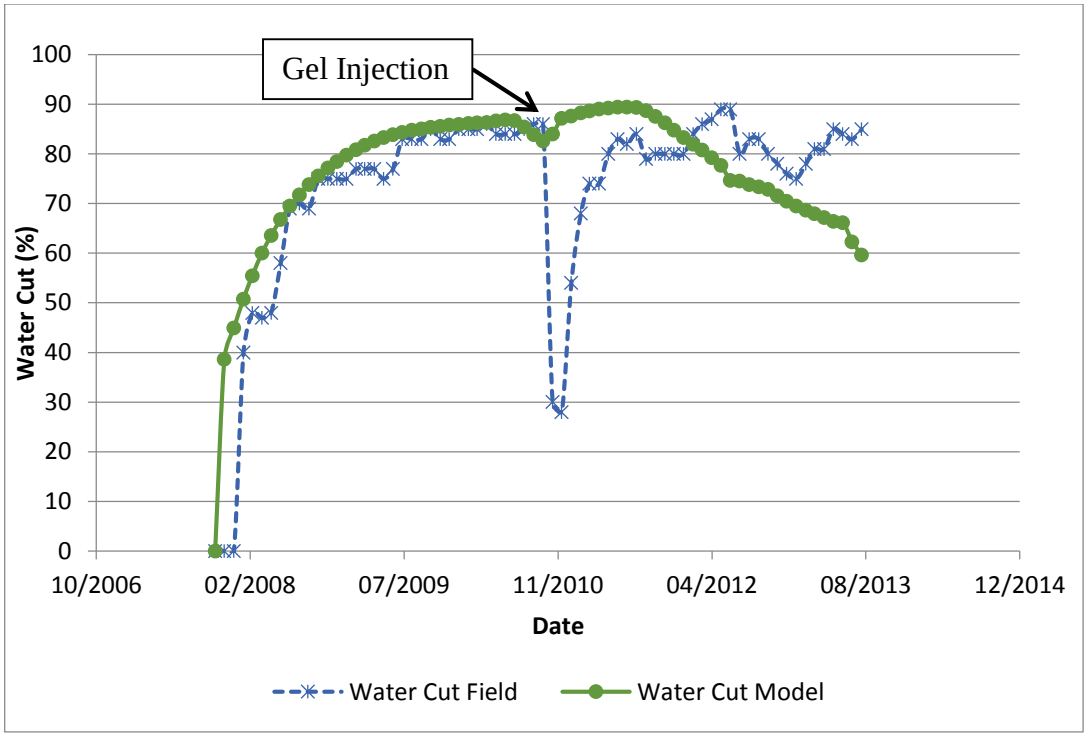

Figure 5-19: Well 231, water cut history

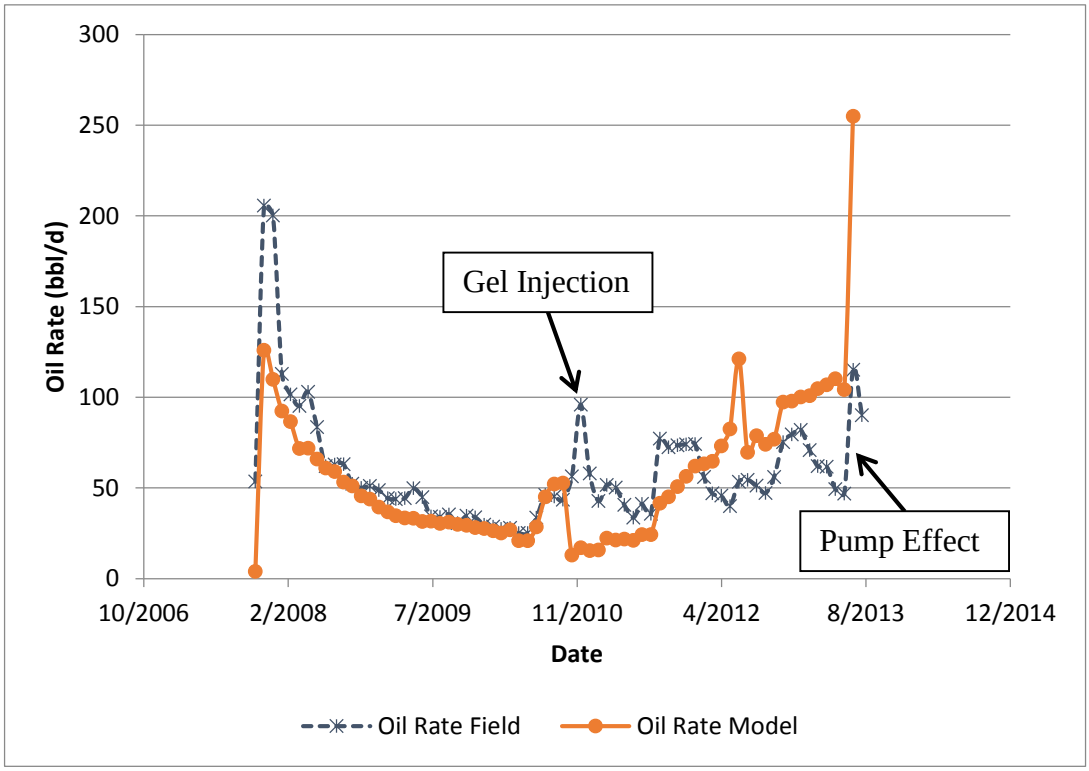

Figure 5-20: Well 231, oil rate history matching

In Table 5-8, reduced chi-square values for goodness-of-fit determination are listed.

Table 5-8: Reduced Chi-Square for goodness-of-fit table

	Reduced Chi-Square	
	Water Rate	Oil Rate
Well 72	0.005	0.536
Well 137	0.423	1.928
Well 230	0.253	0.709
Well 231	0.613	0.909

A glimpse over the curves shows that the trend of simulation and field results in all wells are similar. Likewise, the trend of decreasing in water cut amount during gel injection period is also alike for all wells except well 231. The statistical analysis for determination of goodness-of-fit reveals that the values determined by equation 5-6 are not showing highly significant fit and they are not in accord with error variance. However, to some extent all of the models have fitted the observed field data from moderate fit to high fit. Based on statistical analysis, the trend of descending and ascending of history matching plots especially in the case of water cut data, which is the most important case in water shutoff operation, is in an acceptable range.

5.7 Scenarios

In this section, scenarios based on production history results taken from the CMG STARS's reservoir model are conducted. Alteration in water-cut results is taken into the consideration. Future reservoir behavior focusing on water-cut amount is simulated in the produced reservoir models, and for each well the future behavior in three cases is taken into consideration. In the first case, no gel injection application is considered. In the second case, one or two additional gel injection treatments are conducted with taking gel properties the same as original gel properties. Finally, in the last case, one or two extra gel treatments are conducted when pre-gel treatment amount undergoes 50% increment and polymer gel (Xanthan) treatment amount decreases 50%. The production liquid rates for wells were assigned by STARS based on production history of each well. Accordingly, well 72 was set to produce at average liquid rate of 335 bbl/d; well 137 was assigned to produce at average liquid rate of 150 bbl/d; and wells 230 and 231 were fixed to produce at average liquid rates of 200 bbl/d. It should be noted that, these rates can subject to change during gel injection simulation. The gel injection treatments are taken to be at the same

dates. The dates are chosen to be the July, 2013 and July, 2017. For well 231, since second treatment on the field was implemented in 2012 and modeled in previous section, in order to conform enough timespan one treatment on July, 2017 is conducted. The results for each well are illustrated in Figures 5-21 through 5-24.

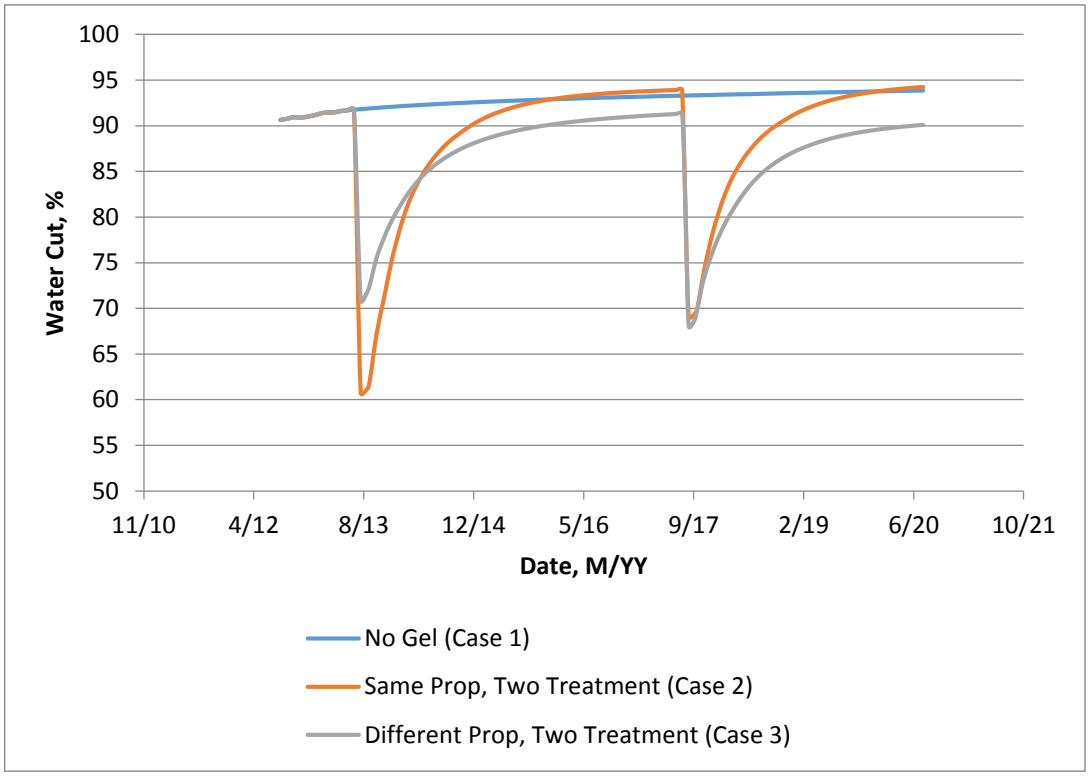

Figure 5-21: Three scenarios for well 72

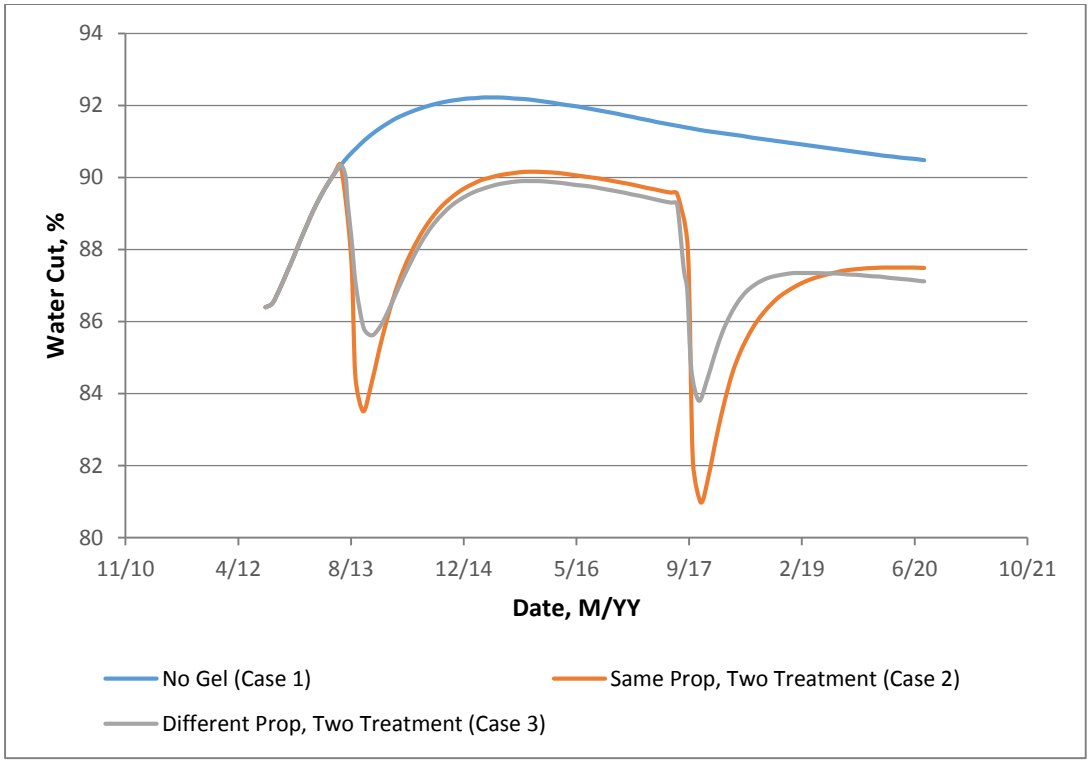

Figure 5-22: Three scenarios for well 137

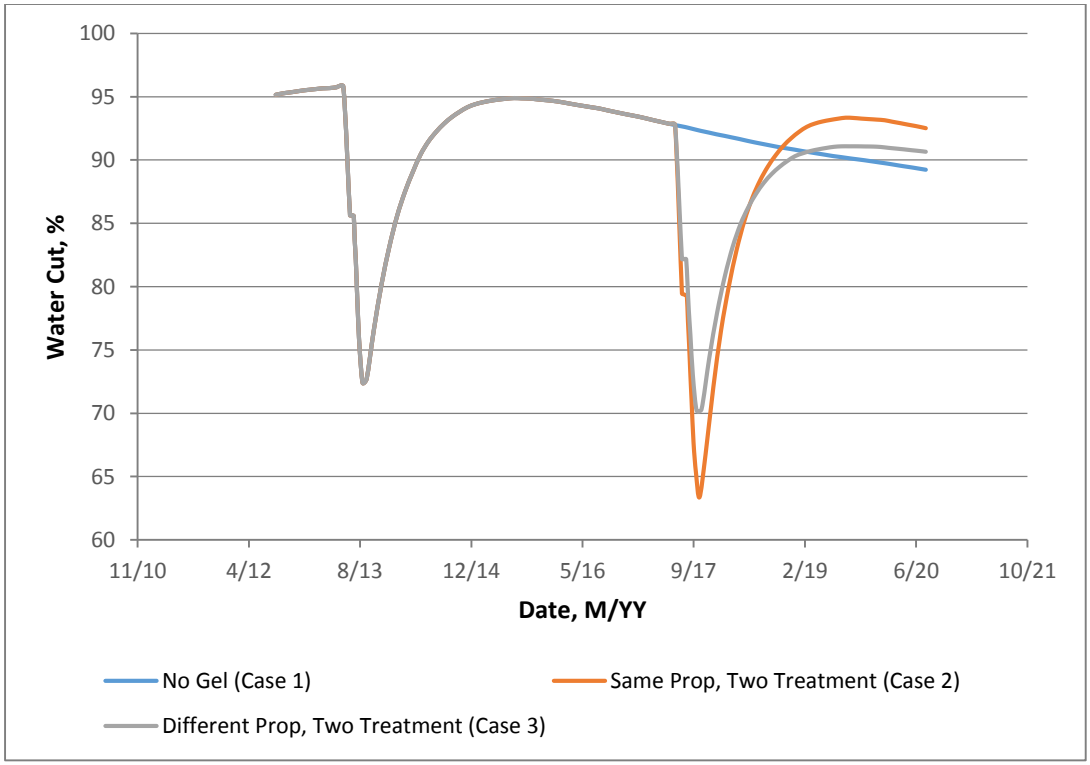

Figure 5-23: Three scenarios for well 230

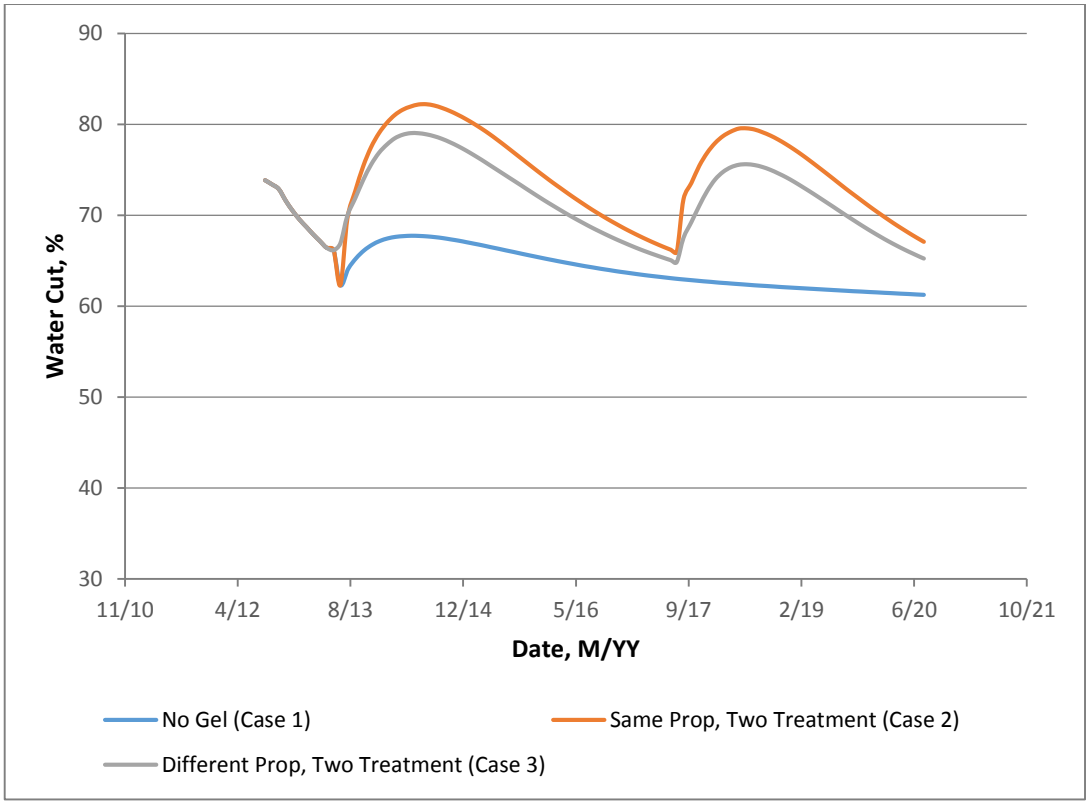

Figure 5-24: Three scenarios for well 231

In ‘case 1’ for all wells, water-cut increases up to certain limit which is about 95%. This limit is not proper for maintaining the economic life of the wells; therefore, periodic application of polymer gel injection must be considered for Field X. Our approach is application of gel injection in period of four years. At the end of each period the water-cut increases to above 90 % in almost all wells and application of gel injection decreases it in a certain level based on well number.

For well 72, ‘case 2’ in the first period water-cut decreases much greater than ‘case 3’. However, in long term ‘case 3’ reveals better results, i.e. less water production. Therefore, changing properties of the gel may decrease the water-cut in produced liquid more significantly; consequently, more oil production is possible if case 3 is used. Similarly, application of ‘case 2’ for well 137 in the short-term for both periods show better results compared to ‘case 3’. However, ‘case 3’ in the long-term shows better results for the well 137. For well 230, both ‘case 2’ and ‘case 3’ shows approximately similar results in short- and long-term; therefore, interpreting the behavior of well after gel injection based on numerical modeling will not be precise.

Well 231 in contrast to other wells shows reverse effect during gel injection, and while other wells produced lower water-cuts during gel injection application water-cut production of this well increases substantially during gel injection. The main reason can be distribution of the fracture sets. Although, the well test calibration of flow through fracture sets for this well is acceptable, deterministic measurements of fracture parameters will be helpful to generate more precise fracture sets.

CHAPTER 6

CONCLUSION AND RECOMMENDATION

Discrete Fracture Network (DFN) modeling and gel injection simulation was conducted on Field X heavy oil reservoir. Geometrical parameters of fracture network are utilized to generate the DFN model. Data from production test of DFN model is calibrated to the actual well test data by adjusting the unknown geometrical parameters until a match was obtained. The fracture properties around each well were then upscaled to assign fracture properties to their neighboring grid of reservoir simulator. Based on available reservoir rock and fluid properties data and properties of injected polymer gel, flow equation was solved numerically according to given initial and boundary conditions in simulator. Reservoir model was generated, subsequently, to provide history match. Finally, scenario study for optimizing the production data was conducted.

Due to lack of geological recorded data and estimated sparse geological parameters, modeling the DFN was based on stochastic data rather than deterministic data. As discussed in chapter 2, availability of cores or exposures scanlines, seismic measurements, and image logging will increase the number of deterministically measured parameters; therefore, the reliability and the accuracy of provided DFN model will be increased. Moreover, production test data is not sensitive and tight enough to be used in calibration analysis. For well 231, well test data calibration provide a match, the history matching and the following scenario results were not in accord with actual data. The reason can be due to the inconsistency of fracture properties and creation of inappropriate fracture distribution which is an outcome of unfitting fracture geological parameters distribution.

On the whole, in this work single well reservoir modeling study is conducted. The results from history matching showed good match for three wells. However, using multi-well modeling based on realistic structural geo-modeling, utilizing deterministically measured fracture parameters for DFN modeling, and accurate production test data for calibration can not only result in more realistic discrete fracture network model, but also better reservoir model and history matching results.

REFERENCES

[1] T. Ahmed, *Reservoir Engineering Handbook*. Elsevier Inc., 2010, pp. 1338–1432.

[2] J. E. Warren and P. J. Root, "The Behavior of Naturally Fractured Reservoirs," *SPE Journal, SPE-426-PA*, vol. 3, no. 3, pp. 245–255, 1963.

[3] M. Karimi-Fard, L. J. Durlofsky, and K. Aziz, "An Efficient Discrete Fracture Model Applicable for General Purpose Reservoir Simulators," *SPE Journal, SPE-88812-PA*, vol. 9, no. 02, pp. 227 – 236, Apr. 2004.

[4] S. H. Lee, M. F. Lough, and C. L. Jensen, "Hierarchical Modeling of Flow in Naturally Fractured Formations with Multiple Length Scales," *Am. Geophys. Union J.*, vol. 37, no. 3, pp. 443–455, Mar. 2001.

[5] R. Juanes, J. Samper, and J. Molinero, "A General and Efficient Formulation of Fractures and Boundary Conditions in the Finite Element Method," *Int. J. Numer. Methods Eng.*, vol. 54, no. 12, pp. 1751–1774, Aug. 2002.

[6] B. Dershowitz, P. Lapointe, T. Eiben, and L. Wei, "Integration of Discrete Feature Network Methods With Conventional Simulator Approaches," *SPE Reserv. Eval. Eng., SPE-62498-PA*, vol. 3, no. 2, pp. 165–170, 2000.

[7] B. Berkowitz, "Characterizing Flow and Transport in Fractured Geological Media: A Review," *Adv. Water Resour. J.*, vol. 25, no. 8–12, pp. 861–884, Aug. 2002.

[8] N. E. Odling, P. Gillespie, B. Bourgine, C. Castaing, J. P. Chiles, N. P. Christensen, E. Fillion, A. Genter, C. Olsen, L. Thrane, R. Trice, E. Aarseth, J. J. Walsh, and J. Watterson, "Variations in Fracture System Geometry and Their Implications for Fluid Flow in Fractured Hydrocarbon Reservoirs," *J. Pet. Geosci.*, vol. 5, no. 4, pp. 373–384, Nov. 1999.

[9] International Society for Rock Mechanics, "Suggested Methods for the Quantitative Description of Discontinuities in Rock Masses," *Int. J. Rock Mech. Min. Sci. Geomech.*, vol. 15, no. 6, pp. 319 – 368, 1978.

[10] O. Kolditz, “Modelling Flow and Heat Transfer in Fractured Rocks: Conceptual Model of a 3-D Deterministic Fracture Network,” *Geotherm. J.*, vol. 24, no. 3, pp. 451–470, Jun. 1995.

[11] E. Hoek and T. Brown, *Underground Excavations in Rock*. London: Transportation Research Broad of the National Academies, 1980, p. 536.

[12] L. Zhang, *Engineering Properties of Rocks*, Fourth. Elsevier Inc., 2005, p. 208.

[13] W. S. Dershowitz and H. H. Herda, “Interpretation of Fracture Spacing and Intensity,” in *The 33th U.S. Symposium on Rock Mechanics (USRMS), 3-5 June, Santa Fe, New Mexico*, 1992, pp. 757–766.

[14] W. S. Dershowitz, “Geometric Conceptual Models For Fractured Rock Masses: Implications For Groundwater Flow And Rock Deformation,” in *ISRM International Symposium - EUROCK 93, 21-24 June, Lisboa, Portugal*, 1993, pp. 71–81.

[15] P. H. S. W. Kulatilake and S. Wang, “Effects of Finite Size Joints on Deformability of Jointed Rock at the Three Dimensional Level,” *Int. J. Rock Mech. Min. Sci. Geomech.*, vol. 30, no. 5, pp. 479–501, Jan. 1993.

[16] P. M. Warburton, “Stereological Interpretation of Joint Trace Data: Influence of Joint Shape and Implications for Geological Surveys,” *Int. J. Rock Mech. Min. Sci. Geomech.*, vol. 17, no. 6, pp. 305–316, Dec. 1980.

[17] L. Zhang and H. H. Einstein, “Estimating the Intensity of Rock Discontinuities,” *Int. J. Rock Mech. Min. Sci.*, vol. 37, no. 5, pp. 819–837, Jan. 2000.

[18] T.-Y. Zhang, M. Zhao, and P. Tong, *Fracture of Piezoelectric Ceramics*, vol. 38. Elsevier Inc., 2002, pp. 147–289.

[19] S. D. Priest, *Discontinuity Analysis For Rock Engineering*, First. London: Chapman & Hall, 1993, p. 473.

[20] G. P. Kruseman and N. A. Ridder, *Analysis and Evaluation of Pumping Test Data*, 2nd ed. International Institute for Land Reclamation and Improvement, Wageningen, Netherlands: Publication 47, 1994, p. 377.

[21] J. Rutqvist, J. Noorishad, C.-F. Tsang, and O. Stephansson, “Determination of Fracture Storativity in Hard Rocks Using High-Pressure Injection Testing,” *Am. Geophys. Union Journal, Pap. number 98WR01863*, vol. 34, no. 10, pp. 2551–2560, 1998.

[22] P. Stafford, L. Toran, and L. McKay, “Influence of Fracture Truncation on Dispersion: A Dual Permeability Model,” *J. Contam. Hydrol.*, vol. 30, no. 1–2, pp. 79–100, Mar. 1998.

[23] J. C. S. Long, J. S. Remer, C. R. Wilson, and P. A. Witherspoon, “Porous Media Equivalents for Networks of Discontinuous Fractures,” *Am. Geophys. Union J.*, vol. 18, no. 3, pp. 645–658, Jun. 1982.

[24] P. Andersson, D. Billaux, V. Cvetkovic, W. Dershowitz, J. Hermanson, A. Poteri, E.-L. Tullborg, and A. Winberg, “TRUE Block Scale Project,” Final Report, Publication No. TR-06-42, Swedish Nuclear Fuel and Waste Management Co, Stockholm, Sweden, 2003.

[25] W. S. Dershowitz, P. R. La Pointe, and T. W. Doe, “Advances in Discrete Fracture Network Modeling Convergence of DFN and Continuum Methods,” in *Proceedings of the 2004 US EPA/NGWA Fractured Rock Conference, Portland*, 2004.

[26] R. S. Seright, R. H. Lane, and R. D. Sydansk, “A Strategy for Attacking Excess Water Production,” in *SPE Permian Basin Oil and Gas Recovery Conference, 15-17 May, Midland, Texas, SPE-70067-MS*, 2001, no. 1, pp. 1–16.

[27] R. R. Reynolds, “Produced Water and Associated Issues,” A Report/Manual for the Independent Operator, Oklahoma Geological Survey, Norman, Oklahoma, 2003.

[28] Golder Associates Team, *Fracman7 Manual*. Golder Associates Inc., 2009.

[29] W. S. Dershowitz and H. H. Einstein, “Characterizing Rock Joint Geometry with Joint System Models,” *Rock Mech. Rock Eng.*, vol. 21, no. 1, pp. 21–51, 1988.

[30] I. Sener, “Methodology Used in Estimating the Raman Reservoir Fracture System Data for Simulation,” in *SPE Annual Technical Conference and Exhibition, 27-30 September, Dallas, Texas, SPE-16978-MS*, 1987.

[31] I. Sener and C. S. Bakiler, “Basic Reservoir Engineering and History-Match Fractured Raman Reservoir, Turkey,” in *Middle East Oil Show, 11-14 March, Bahrain, SPE-17955-MS*, 1989, pp. 255–266.

[32] C. R. Berg, “The Effect of Fracture and Borehole Orientation on Fracture Frequency and Density,” 2012. [Online]. Available: http://www.resdip.com/docs/fracture orientation.pdf. [Accessed: 19-Jan-2015].

[33] P. F. Wallis and M. S. King, “Discontinuity Spacings in a Crystalline Rock,” *Int. J. Rock Mech. Min. Sci.*, vol. 17, no. 1, pp. 63–66, 1980.

[34] E. Villaescusa and Y. Potvin, “Ground Support in Mining and Underground Construction,” in *Proceedings of the Fifth International Symposium on Ground Support 28-30 September 2004, Perth, Western Australia*, 2004, vol. 23, p. 659.

[35] H. H. Einstein, G. B. Baecher, and D. Veneziano, “Risk Analysis for Rock Slopes in Open Pit Mines,” Final Technical Report, Publication No. R80-17, Order No. 669, Dept. of Civil Eng., Massachusetts Institute of Technology, Cambridge, Massachusetts, 1980.

[36] J. Kemeny and R. Post, “Estimating Three-Dimensional Rock Discontinuity Orientation from Digital Images of Fracture Traces,” *J. Comput. Geosci.*, vol. 29, no. 1, pp. 65–77, Feb. 2003.

[37] A. Niemi, K. Kontio, A. Kuusela-Lahtinen, and A. Poteri, “Hydraulic Characterization and Upscaling of Fracture Networks Based on Multiple-Scale Well Test Data,” *Am. Geophys. Union Journal, Pap. No. 2000WR900205*, vol. 36, no. 12, pp. 3481–3497, Dec. 2000.

[38] X. Wang and A. Ghassemi, “A Three-Dimensional Stochastic Fracture Network Model for Geothermal Reservoir Stimulation,” in *Thirty-Sixth Workshop on Geothermal Reservoir Engineering Stanford University, Stanford, California, January 31 - February 2, 2011*, 2011, no. 1996.

[39] Computer Modeling Group Ltd., *STARS, Advanced Process and Thermal Reservoir Simulator User’s Guide*. Calgary: Computer Modeling Group Ltd., 2007, pp. 1–1018.

[40] K. Kazemi, L. S. J. Merrill, K. P. Potterfield, and P. R. Zeman, “Numerical Simulation of Water-Oil Flow in Naturally Fractured Reservoirs,” *SPE Journal, SPE-5719-PA*, vol. 16, no. 6, pp. 317–326, 1976.

[41] A. C. Hill and G. W. Thomas, “A New Approach for Simulating Complex Fractured Reservoirs,” in *Middle East Oil Technical Conference and Exhibition, 11-14 March, Bahrain, SPE-13537-MS*, 1985, pp. 429–436.

[42] J. R. Gilman and H. Kazemi, “Improvements in Simulation of Naturally Fractured Reservoirs,” *SPE Journal, SPE-10511-PA*, vol. 23, no. 04, pp. 695 – 707, 1983.

[43] M. Demir, N. N. Topgüder, M. Yilmaz, Y. Karakeçe, Y. Ince, and U. Karabakal, “Water Shutoff Gels Improved Oil Recovery in Naturally Fractured Raman Heavy Oilfield,” in *SPE Russian Oil & Gas Technical*

Conference and Exhibition held in Moscow, Russia, 28-30 October 2008, SPE-116878, pp. 1–11.

[44] M. Honarpour, L. Koederitz, and A. H. Harvey, *Relative Permeability of Petroleum Reservoir*. Boca Raton: CRC Press, 1986, p. 143.

[45] T. D. van Golf-Rakht, *Fundamentals of Fractured Reservoir Engineering*. Netherlands: Elsevier Inc., 1982, p. 710.

[46] S. Akin, "Estimation of Fracture Relative Permeabilities from Unsteady State Corefloods," *J. Pet. Sci. Eng.*, vol. 30, no. 1, pp. 1–14, Jun. 2001.

[47] M. Izadi, S. R. Shadizadeh, and S. Moradi, "Experimentally Measurements of Relative Permeability in Fractured Core," *Int. J. Sci. Emerg. Tech.*, vol. 3, no. 1, pp. 46–51, 2012.

[48] S. M. Fatemi, R. Kharrat, and S. Vossoughi, "Investigation of Top-Down In-Situ Combustion Process in Complex Fractured Carbonate Models : Effects of Fractures' Geometrical Properties," in *Canadian Unconventional Resources Conference*, 2011, pp. 1–21.

[49] E. C. Robertson, "Thermal Properties of Rocks," Open-File Report, Publication No. 88-441, U.S. Department of Interior Geological Survey, Reston, Virginia, 1988.

[50] A. J. Mansure, "Hot Oiling Spreadsheet," Technical Report, Publication No. 96-2247, Sandia National Labs., Albuquerque, New Mexico, United States, 1996.